IEEE Access
Multidisciplinary | Rapid Review | Open Access Journal

Received August 25, 2021, accepted September 11, 2021, date of publication September 17, 2021, date of current version October 1, 2021.

Digital Object Identifier 10.1109/ACCESS.2021.3113857

Likelihood Estimation and Wavelet Transformation Based Optimization for Minimization of Noisy Pixels

ARVIND DHAKA[1], AMITA NANDAL[1], HAMURABI GAMBOA ROSALES[2], HASMAT MALIK[3], (Senior Member, IEEE), FRANCISCO ENELDO LOPEZ MONTEAGUDO[2], MONICA I. MARTINEZ-ACUNA[4], AND SATYENDRA SINGH[5], (Member, IEEE)

[1]Department of Computer and Communication Engineering, Manipal University Jaipur, Jaipur, Rajasthan 303007, India
[2]Unidad Academica de Ingenieria Electrica, Universidad Autonoma de Zacatecas, Zacatecas 98000, Mexico
[3]Berkeley Education Alliance for Research in Singapore (BEARS), University Town, NUS Campus, Singapore 138602
[4]Faculty of Chemical Sciences, Autonomous University of Zacatecas (UAZ), Zacatecas 98000, Mexico
[5]School of Electrical Skills, Bhartiya Skill Development University, Jaipur 302037, India

Corresponding authors: Hasmat Malik (hasmat.malik@gmail.com) and Amita Nandal (amita_nandal@yahoo.com)

This work was supported in part by the Universidad Autonoma de Zacatecas, Mexico, through the Consejo Nacional de Ciencia y Tecnología (CONACYT) Mexico.

ABSTRACT In recent times the statistical computation techniques are gaining a lot of interest for analyzing the behavior of various mathematical distributions. This paper derives the likelihood distribution of image priors which has been further used to denoise the image. This paper aims to maximize the likelihood estimation of the parameters of interest i.e. prior and posterior estimation. We have proposed a prior-based distribution model which has been applied to additive, multiplicative and mixed noise cases. The various estimation parameters such as statistical variance and mean parameters have been used to evaluate the maximum likelihood of image priors for these noise models. Later, we have used an optimization technique based on the likelihood to reconstruct noise-free images efficiently. This paper uses conditional likelihood and wavelet transformation-based minimization techniques to minimize the noise in the pixels and a final denoised image is recovered. The conditional likelihood of the image has been optimized using pixel-based minimization w.r.t. the wavelet transformation coefficients. The simulation and analytical results have also been presented for the different noise cases.

INDEX TERMS Gamma, Gaussian and Poisson distributions, image priors, log-likelihood estimator, normalization and minimization, noise models, posterior estimate, wavelet transformation.

I. INTRODUCTION

The image denoising methods have gradually developed from spatial domain methods to transform domain methods. Over the years, Fourier transform domain methods have been extensively used and gradually other methods have emerged such as cosine transform, wavelet transform, and block-matching and 3D filtering [1]–[4] methods for image recovery. One of the advantages of using the wavelet transform domain method is that in this method the characteristics of image information and noise are different. Thus, image characteristics are well preserved, regardless of its frequency content. This paper proposes a parametric estimation technique to get a unique solution from the various noise image models so that a clean image can be retrieved.

The parametric estimation techniques are used to estimate the parameters of a distribution model which maximizes the fit to a particular data set. The most common techniques used in mathematical statistics are maximum likelihood estimation (MLE) [5] and Bayesian estimation (BE) [6]. These techniques return the prior and posterior distribution of the parameters, where the mean of the posterior distribution is the best-fitting estimate of the parameters. The conjugate priors have been defined in form of a log-likelihood function. This log-likelihood function is a form of simple standardized function of parameters whose multiplication with the prior distribution yields an exponential distribution.

The associate editor coordinating the review of this manuscript and approving it for publication was Yong Yang.

Such distribution can be used to model the noise in any image and eventually be used to enhance the image quality [7]–[9]. This paper has various advantages over other existing studies. In modern image denoising techniques sparse signal representation has been used for linear and nonlinear transformations. In the existing studies, the pixel intensity or noise variance has been analyzed rather than the actual noise distribution [10]. It is evident that noise distribution greatly affects the performance of any denoising algorithm [11]. Therefore, this paper provides a detailed analysis of noise models using likelihood estimation. In this paper, different noise models have been statistically estimated using the likelihood of image priors. We have also performed posterior analysis by calculating the bias and accuracy of the proposed algorithm. In the proposed methods the priors have not only been used to define the parametric limits but also provide an accurate statistical posterior analysis for various noise distributions. By simulating individual samples of posteriori distribution, the true parameter values can be recovered which is assessed using the mean and median of the expected distribution. These estimates are then used to compute the accuracy and reliability of the point estimations obtained using statistical parameters.

This paper proposes a denoising method that is capable of removing the noise from an image without affecting image details using likelihood estimation. Image denoising using wavelet transform is gaining popularity due to its sparsity and multiresolution. This paper proposes a parametric estimation technique considering three noise models i.e. additive, multiplicative, and mixed noise models. Since we cannot get a unique solution from the noise image models to retrieve the clean image. Therefore, the image denoising method has to be used for a good estimation of a clean image. Spatial domain and transform domain methods are extensively used as denoising methods. The proposed method is based on the transform domain method. The transform domain methods are advantageous than spatial domain methods because in spatial domain methods somehow the noise is eliminated but due to image blurring the image loses edge sharpness. The proposed methods also analyze the accuracy of the noise model. Firstly, we calculate the conditional likelihood of noisy image w.r.t. noise-free image. Then, we maximize the likelihood equation w.r.t. bivariate conjugate priors of image i.e. mean and variance because these image priors are less susceptible to variations in pixel intensity, thus yields accuracy and reliability of the proposed algorithm. Moreover, the likelihood estimation improves robustness and reduces bias before the final reconstruction of noise-free images. Further wavelet transform has been optimized by minimizing the noisy pixels in the image to reconstruct noise-free image. Finally, inverse wavelet transform computes the final denoised image.

In this paper, we have employed norm-based optimization and usually, it is expected to maximize the PSNR of the result which can be observed from the qualitative and quantitative results. As such, using the norm-based optimization has proven to provide better results on other quality evaluation metrics are also mentioned in this paper.

Optimization helps to solve a problem by tuning a set of parameters to achieve an optimal solution. The optimization functions could be associated with a real-life problem, and have endless applications. In this paper, we decided to use optimization for the minimization of noisy pixels. In the proposed method the set of parameters are transformation coefficients and transformed noise-free pixels only. The optimal goal is noise-free image reconstruction whose quality is assessed in terms of various performance metrics. In the proposed method we have used discrete gradients of the image and it is well-known fact that norm-based optimization is capable of representing the sparsity of the gradient image better and preserves the edge.

The contributions of this paper are as follows-

1. The wavelet based methods presented in the literature had a problem of the biased estimate of their wavelet coefficient. In this paper, we have removed the bias from wavelet coefficients based on the fact that bias in the scaling coefficient is scaling independent.
2. The noise-free signals are estimated using magnitude data points. The controversial point is that due to neighborhood smoothing using MLE the sharpness of edges and fine structure degrades. In this paper, we have addressed this problem as the proposed method possesses a high degree of redundancy in the context of images and assures that pixels have a similar neighborhood which is achieved by computing horizontal and vertical gradients for different noise distributions i.e. Gaussian, Gamma, and Poisson.
3. We use mean and variance-based image priors for maximizing the likelihood to locate the neighborhood pixels for noise-free pixel estimation.
4. The proposed method is different from the methods presented in the literature because this work is focused on estimating the noise-free image with the use of priors and log-likelihood criteria. Later, wavelet coefficients are used to calculate likelihood-based transformation.
5. Finally, we present a unique solution to the optimization problem for the non-quadratic and non-smooth log-likelihood problem to yield a noise-free image.
6. We generalize the norm-based optimization for noise-free image reconstruction. The proposed model can achieve superior performance compared with the existing related methods for multiple reasons. Firstly, due to the norm regularization term, the proposed model can reduce streak artifacts. Secondly, due to the -norm regularization term, the smoothing is improved and the proposed model is proven to be better edge-preserving and to provide a better sparsity representation. We have used the optimization algorithm in such a way that its algebraic framework solves the optimization effectively using the minimization problem.

The rest of the paper is organized as follows; Section II provides the literature review. Section III details the proposed method with wavelet-based pixel transformation and final image recovery. Various performance measures are provided in Section IV. Section V presents numerical results and discussions. Finally, Section VI concludes the paper.

II. BACKGROUND

Noise modeling requires parametric distributions with certain physical or empirical considerations and denoising requires an estimate of the statistics of these parameters. Various denoising techniques have been proposed in the image processing literature over the years [7]–[10]. Bayesian methods are used frequently due to their adaptability to various noises [6]. A Bayesian framework interprets the obtained image as an accumulation of the original image. By adding any prior knowledge of the signal, a Bayesian denoising technique is formed and thus the formulated Bayesian method treats denoising as an estimation problem. In [12], [13] the additive white Gaussian Noise (AGWN) based model is used for estimating the multiplicative noise model, but the final image resolution is degraded. This resolution problem can be overcome by using image priors. In another work, Markov random field (MRF) [14] based denoising framework has been developed for an estimation which is based on image priors and minimization of the energy function. The selection of a suitable prior is very important for preserving the image structure and incorporating smoothness in the denoised image. In recent years, for image denoising, the Gaussian mixture models (GMM) [15], [16] have been developed and they can represent image priors as well.

Another challenge in image denoising problems is to retrieve the original uncorrupted image efficiently. As per the literature, log-likelihood based estimation is most commonly used in image denoising. There exist literature that introduced the priors to likelihood distributions such as GMM prior [17]. The reason to use priors in image denoising is that it can provide Maximum A-posteriori (MAP) based statistical estimation [18] using some regularization parameters of images. Based on this idea, a Bayesian framework based Expected Patch Log Likelihood (EPLL) algorithm [20] has been proposed to model the probability of image patches using Gaussian Mixture Model (GMM). Also, the various noise hypotheses can be models easily using maximum likelihood estimation (MLE) [21]. The limitations of MLE are poor neighborhood smoothing, partial restoration of image structure, and inefficient preservation of edge sharpness. This MLE estimate does not guarantee accurate statistics. In recent years, the Maximum A-posteriori (MAP) model proved to satisfy various analytical and computational properties for efficient estimation. The MAP estimation is also dependent on the posterior log-likelihood function [22]–[25]. In [22], a denoising model (VMAP) based on variational approaches has been presented which proved to maximize the posterior distribution of the image. The posterior distribution of the image was computed using the Bayes formula-based random field model [26]. However, the random field models have observed some implementation problems while choosing the parameters of interest.

In [27], Bayesian hyper-parameter estimation (BHE) was used which was based on factorized priors. But, when the image size was small there was some inconsistent observation. These inconsistencies have been removed in this paper by using likelihood-based estimation and prior model.

In the context of the computational difficulties of exponential distributions, a new sub-pixel classification algorithm (SCA) was introduced where prior information is expressed in terms of the occurrence probabilities in a pixel [28]. This is evident that the performance of the algorithm can be significantly improved by incorporating prior information. We have used priors with likelihood estimation which has improved the bias and accuracy.

A Bayesian multi-scale method (BMM) was proposed for multiplicative speckle noise removal [29]. This method uses a wavelet transform domain and a gamma distribution based prior to capture the heavy-tailed nature of wavelet coefficients. This method lacks to optimize the noise-free wavelet coefficients. In the proposed method by exploiting the prior together with a Gaussian/ Gamma/ Poisson likelihood, an analytical wavelet function is used which achieves a better estimate of noise-free wavelet coefficients.

Wavelet coefficients based hidden bayesian network (HBN) was proposed to model the prior probability of the original image [30]. This method uses a MAP estimator to retrieve the denoised wavelet coefficients. This method is highly complex because each wavelet coefficient is modeled as a hidden state variable. The proposed method uses prior information for likelihood estimation and later wavelet coefficient based optimization problem is solved to get the denoised image. From literature [24], it is well known that prior estimate is a natural and optimal choice when the PDF of signal and noise are known. In this paper, we have used Jeffrey's conjugate prior [31], [32].

In [33] a Variational Bayesian Approach (VBA) is proposed for Image Restoration Poisson–Gaussian Noise. The Bayesian framework is based on Markov Chain Monte Carlo (MCMC) sampling algorithms. But despite the good estimation performance that has been obtained, such methods remain computationally expensive for large-scale problems. Moreover, the comparisons with image deblurring methods are dedicated to a pure Poisson noise model. They were observed to lead to poor results in terms of restoration quality and to present a high computational time. This limitation is overcome in the proposed method using minimization-based regularization parameters which reduces the account of noisy pixels directly and yields high-quality restored image.

In [34] an imaging framework has been defined for image restoration of images corrupted by Poisson noise followed by

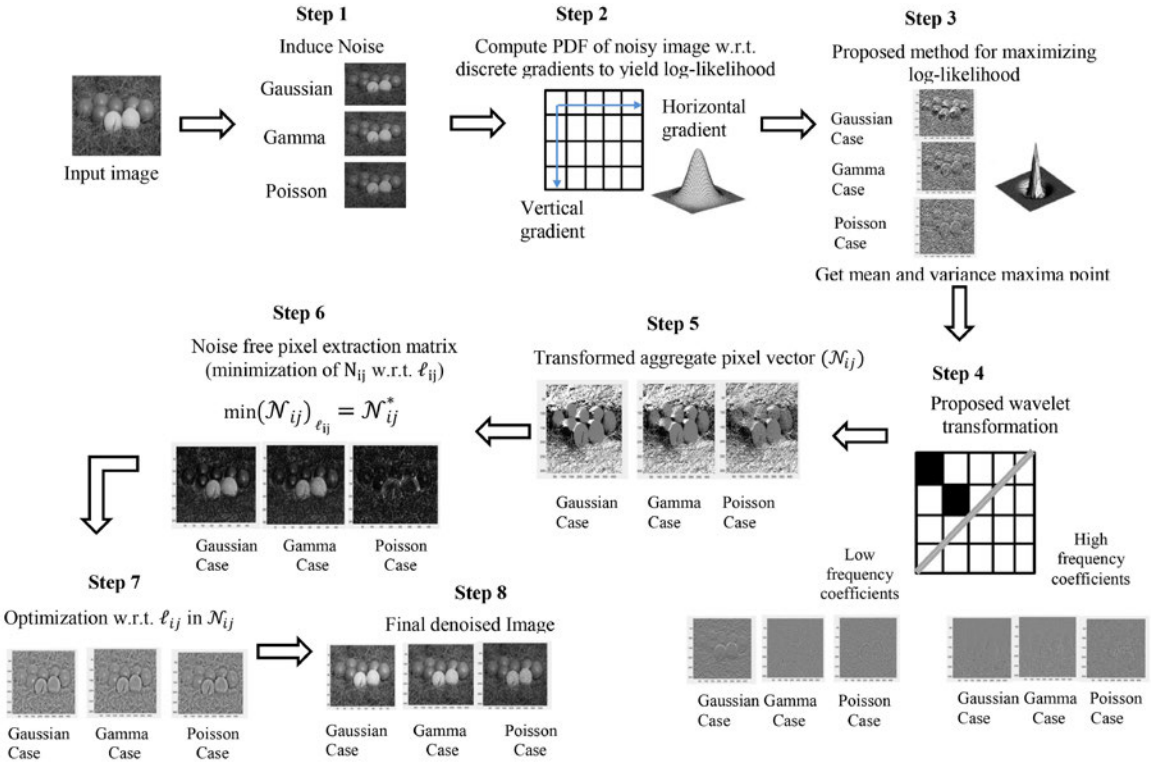

FIGURE 1. Block diagram showing the steps followed in proposed methodology.

additive Gaussian noise using alternating direction method of multipliers (ADM) optimization algorithm. One of the limitations of their method is that it is sensitive to variance of the likelihood estimate because the upper bound on step size of this optimization algorithm is the inverse data likelihood. Moreover, if a restriction is applied to step size by keeping it low then the gradient of the log-likelihood increases exponentially with the intensity of the measured image. Therefore the empirical convergence rate becomes low. This limitation is not present in the proposed method because we have used norm-based optimization. However, the method presented in [34] is quite faster in computation as compared to the proposed method.

The optimization problems involved in image restoration applications are usually difficult due to the non-differentiability of the norm and the high dimensionality of the image data. In the past several decades, various approaches have been proposed such optimization method for maximization of statistical estimate [35], [36], the second-order cone optimization method [37], [38] the fixed-point iterative method [39], and other methods [40]–[44]. These methods are capable of denoising the image but they lack numerical stability. Therefore, we have used norm-based optimization algorithm in this paper.

In this paper, the performance of the proposed method has been evaluated in terms of bias accuracy for varying image sizes. The simulation results are well compared with the conventional techniques [21], [22], [27]–[30], [33], and [34]. The proposed estimation depends upon the prior distribution and its ability to extract noise. This paper uses the wavelet transformation [42] to represent the image pixels as high and low-frequency wavelet coefficients. Later, these coefficients are used for our minimization problem. Thus, one of the important aspects of this paper is that by choosing appropriate prior value the noise extraction can be improved and image details can be preserved efficiently.

III. PROPOSED METHODOLOGY

Noise affects the information pixels in an image which can remove fine structural details under general conditions. The real-life noises are much more complex than the considered noise distribution models. But, for the analysis purpose, the noise distribution model should be considered such that an approximate solution is obtained from the noisy image to obtain the clean image. Therefore, there is a need to choose a distribution model. We have used the distribution models that represent additive, multiplicative, or mixed noise models. The discrete gradients of these distribution models give probability density functions which are maximized using maximum likelihood condition and image priors. These estimated values image priors i.e. mean and variance is used to maximize the probability functions which have been represented mathematically. Figure 1 details the steps of the proposed methodology which is mathematically illustrated in later sections. We have presented the stage-wise image restoration results for one image in Figure 1 to analyze the

quality of the image. Later, in this paper, the numerical results have also been presented for different stages of the proposed methodology which indicates the values of various performance metrics.

The noise is induced in the input image that follows a noise model. The noise model is defined by representing the image in discrete form. Consider a sampling space $\mathbb{S}$ which consists of possible outcomes of a random experiment. This sampling space defines the discrete form of the model. Let us assume resolution control of image as $r > 0$. The discrete image (I) of size $M \times N$ is given as matrix $I = [I_{ij}]$, such that $i = 0, 1, 2, \ldots M-1$ and $j = 0, 1, 2, \ldots, N-1$. The intensity values of the discrete image lie in a range between 0 to 255 such that the pixel location (ir, jr) has horizontal and vertical distance r with a pixel grid $x_{ij} = (ir, jr)$. The intensity noise is dependent on each pixel location and the observed noise depends on the surrounding pixels.

A. GAUSSIAN NOISE MODEL: CASE1

For the Gaussian noise model, the discrete image I with $M \times N$ matrix realization is represented in terms of noisy image as $I^a = I + a|g|$ In this case we assume that a is Gaussian distributed random variable which is responsible for Gaussian intensity noises. Here, $a = a_{ij}$ is the noise related to every pixel. $|g|$ is a matrix of the norm of discrete gradients. For every pair (i, j) in the set we assign a discrete gradient g_{ij} of I at x_{ij} by

$$g_{ij} = \frac{1}{r}\begin{pmatrix} I_{i+1,j} - I_{ij} \\ I_{i,j+1} - I_{ij} \end{pmatrix}. \tag{1}$$

The resultant of g represents a matrix of the norm of discrete gradient $|g_{ij}| \rightarrow |g|$. We can now separate the discrete gradient $|g|$ of a discrete image from horizontal and vertical discrete gradients $\nabla_h I$ and $\nabla_v I$ respectively of image I which are written as

$$\nabla_h I\left(x_{ij}\right) = \frac{1}{r}\begin{pmatrix} I\left(x_{i+1,j}\right) - I(x_{ij}) \\ I\left(x_{i,j+1}\right) - I(x_{ij}) \end{pmatrix}, \tag{2a}$$

$$\nabla_h I\left(x_{ij}\right) = \frac{1}{r}\begin{pmatrix} I\left(x_{i,j+1}\right) - I(x_{ij}) \\ I\left(x_{i+1,j}\right) - I(x_{ij}) \end{pmatrix}. \tag{2b}$$

To approximate the intensity noise model, we assume that the overall shift in gradient which is written as $\nabla I\left(x_{ij}\right)$ such that $\nabla I\left(x_{ij}\right) = \sqrt{\nabla_h I\left(x_{ij}\right)^2 + \nabla_v I\left(x_{ij}\right)^2}$. Now the pixel grid becomes

$$x_{ij}^a = x_{ij} + a_{ij}\frac{\nabla I\left(x_{ij}\right)}{\left|\nabla I\left(x_{ij}\right)\right|}. \tag{3}$$

In eq. (3) the discrete gradients are Gaussian distributed probability density function (PDF) [12], [23].

1) PRIOR AND GAUSSIAN NOISE DISTRIBUTION

As per literature [24], when the noise and PDF of the image signal are known then the prior estimate is one of the optimal choices for any denoising algorithm. Let us assume the Gaussian distribution as two parameters exponential family which is represented in form of the probability density function ($p(.)$) as

$$p\left(I^a, \mu, \sigma^2\right) \propto \left(\sigma^2\right)^{-\frac{1}{2}} e^{-\frac{1}{2\sigma^2}(I^a-\mu)^2}. \tag{4}$$

In eq. (4) we need to have both mean (μ) and variance $\left(\sigma^2\right)$ as random variables to obtain bivariate conjugate prior. We use two cases to build up image priors in terms of variance and known mean. Eq. (4) depicts the dependency of distribution on μ. The Gaussian density is un-normalized which is represented using the exponential of the negative of the quadratic form in μ. The product of two such factors is also an un-normalized Gaussian density i.e. the conjugate prior of μ [26]. Let us assume the probability density function from point of view of mean and variance of prior as

$$p\left(I^a \mid \mu_0, \sigma_0^2\right) \propto \left(\sigma_0^2\right)^{-\frac{1}{2}} e^{-\frac{1}{2\sigma^2}(I^a-\mu_0)^2}. \tag{5}$$

Here, μ_0, σ_0^2 are mean and variance of the prior. Now consider Gaussian distribution from point of view of mean and variance as

$$p\left(I^a|\mu, \sigma^2\right) \propto \left(\sigma^2\right)^a e^{-\frac{b}{\sigma^2}}. \tag{6}$$

Here, $a = -\frac{1}{2}$, $b = \frac{1}{2}\sum_{i=0}^{M-1}\sum_{j=0}^{N-1}\left(I_{ij}^a - \mu\right)^2$. Eq. (6) is another form of Gamma distribution, but the random variable σ^2 is in the denominator rather than the numerator in the exponential term. It is assumed that prior distribution for variance is an inverse Gamma distribution in terms of the hyper-parameters which can be written as

$$p\left(\sigma^2|\alpha, \beta\right) = \frac{\beta^\alpha}{\Gamma(\alpha)}\left(\sigma^2\right)^{-\alpha-1} e^{-\frac{\beta}{\sigma^2}}. \tag{7}$$

$\alpha\beta$ are hyper-parameters [45]. Now the images can be modeled using the random vectorbased realization of the prior distribution. For sample test data, the noisy variants of images have been used and random noise has been artificially distributed in images. Due to the random noise inclusion, the probability distribution of norms of discrete gradients of intensities is needed [28]. This probability distribution is concentrated around zero which ensures the dominant flat region of the image. We consider histogram of $|g|$ to derive image priors using an appropriate probability density function. We assume that probability $p(I)$ depends on the matrix $|g|$ of I. These discrete gradients are independent and identically distributed. So, the probability density of I is the product of derivatives of g_{ij}. The absolute values of Gaussian distributed discrete gradients in case of prior is written as

$$p\left(I^a|\mu_0, \sigma_0^2\right) \propto Ce^{-\frac{1}{2\sigma_0^2}\sum_{i=0}^{M-1}\sum_{j=0}^{N-1}(g_{ij})^2}. \tag{8}$$

Here, $C = \left(\sigma_0^2\right)^{-\frac{1}{2}}$. To generalize the definition for non-discrete cases, we define maximum A-posteriori estimation for discrete random vectors using conditional

probability [23]. We define conditional probability which is written as

$$p\left(I|I^a\right) = \begin{matrix} \frac{p(I,I^a)}{p(I^a)} \\ 0, \, if \; p\left(I^a\right) = 0 \end{matrix}, \, if \; p\left(I^a\right) > 0. \tag{9}$$

The mapping $I^a \rightarrow I^0 := \underset{I}{argmax}\, p(I|I^a)$ is called maximum A-posteriori (MAP) estimator and I^0 is a MAP estimate function [23]. We have I^a a noisy image that is distorted by one of the noise processes. I is associated with one of the image priors. The probability density function for Gaussian intensity noise is written as

$$p\left(I^a|I\right) = \frac{1}{\sigma\sqrt{2\pi}} \prod\nolimits_{\forall i,j} \exp\left(-\frac{\left(I^a_{ij}-\mu\right)^2}{2\sigma^2}\right). \tag{10a}$$

By simplifying,

$$-\log p\left(I^a \mid I\right) = \log\left(\sigma\sqrt{2\mu}\right) + \sum\nolimits_{\forall i,j} \frac{\left(I^a_{ij}-\mu\right)^2}{2\sigma^2}. \tag{10b}$$

The main goal of the posterior estimate is to retain I by maximizing the product of conditional probability density $p\left(I^a|I\right) = \prod_{\forall i,j} p\left(I^a_{ij}|I\right)$. The probability density of I is given by its image prior $p\left(I\right)$. This maximization is equivalent to the minimization of the negative logarithm of conditional probability density. Mathematically

$$-\log\left(p\left(I\right)\right) = \sum\nolimits_{\forall i,j} \frac{1}{2\sigma_0^2}\left|\left(g_{ij}\right)^2\right|. \tag{11}$$

In terms of discrete gradients,

$$p\left(I^a|I\right) = \frac{1}{\sigma\sqrt{2\pi}} \sum\nolimits_{\forall i,j} \frac{1}{|g_{ij}|}.exp\left(-\frac{\left(I^a_{ij}-\mu\right)^2}{2\sigma^2\left|g_{ij}\right|^2}\right). \tag{12}$$

2) MAXIMIZATION OF LIKELIHOOD ESTIMATION

The loglikelihood estimate for Gaussian distribution [25] is calculated as,

$$\mathbb{L}_{gaussian}\left(\mu,\sigma^2|I^a\right) = \log\left[\left(\frac{1}{\sigma\sqrt{2\pi}}\right)^{M+N} \prod\nolimits_{\forall i,j} e^{\frac{-\left(I^a_{ij}-\mu\right)^2}{2\sigma^2}}\right]. \tag{13}$$

The maximum likelihood condition is calculated using differentiation of eq. (13) w.r.t. mean (μ) and variance (σ^2). This differentiation is equated to zero for calculating the maxima point.

$$\frac{d}{d\mu}\left(\mathbb{L}_{gaussian}\left(\mu,\sigma^2|I^a\right)\right) = \frac{d}{d\mu}\left[-MN\log\left(\sigma\sqrt{2\pi}\right)\right] - \sum_{\forall i,j}\frac{d}{d\mu}\left[\frac{-\left(I^a_{ij}-\mu\right)^2}{2\sigma^2}\right] - \sum_{\forall i,j} I^a_{ij} + MN\mu = 0, \tag{14a}$$

$$\hat{\mu} = \frac{1}{MN}\sum_{\forall i,j} I^a_{ij}. \tag{14b}$$

$$\frac{d}{d\sigma^2}\left(\mathbb{L}_{gamma}\left(\mu,\sigma^2|I^a\right)\right) = \frac{d}{d\sigma^2}\left[-MN\log\left(\sigma\sqrt{2\pi}\right)\right] - \sum_{\forall i,j}\frac{d}{d\sigma^2}\left[\frac{-\left(I^a_{ij}-\mu\right)^2}{2\sigma^2}\right], \tag{15a}$$

After simplification,

$$\widehat{\sigma^2} = \frac{1}{MN}\sum_{\forall i,j}\left(I^a_{ij}-\hat{\mu}\right)^2. \tag{15b}$$

Eq. (13) is maximized at mean and variance which is written in eq. (14b) and eq. (15b) respectively. This estimate has also been used to compute bias [28].

B. GAMMA NOISE MODEL: CASE 2

The discrete image I with $M \times N$ matrix realization can be represented in terms of Gamma noise as $I^a = Ia\,|g|$ This is the case for multiplicative noise which is modeled using Gamma distribution [29]. In this case, let us consider that a is Gamma distributed random variable which is responsible for multiplicative noise. $|g|$ is a matrix of the norm of discrete gradients. Gamma density function with respect to a and g is given as

$$f\left(I^a|g,a\right) = \begin{matrix} \frac{I^a}{\Gamma(I^a)}.I^{(g-1)}.\exp\left(-gI^a\right), \; if \; I^a \geq 0 \\ 0, \; otherwise. \end{matrix} \tag{16}$$

$\Gamma\left(.\right)$ denotes Gamma function.

1) PRIOR AND GAMMA NOISE DISTRIBUTION

Let us consider Gamma distribution in terms of mean and variance whose PDF function [30] is written as

$$p_{gamma}\left(\mu,\sigma^2\right) = \frac{\left(\sigma_0^2\right)^{\mu}\left(\sigma^2\right)^{\mu-1}}{\Gamma\left(\mu\right)}\exp\left(\sigma_0^2\sigma^2\right). \tag{17}$$

The density function [32] of image I^a is written as

$$p\left(I^a\right) = \int N\left(I^a;0,\sigma^2\right)p_{gamma}\left(\mu,\sigma^2\right)d\sigma^2. \tag{18}$$

$N\left(I^a;0,\sigma^2\right)$ is Gaussian distribution of argument $I^a\mu$ and σ^2

The marginal PDF of I^a is given

$$p_{marginal}\left(I^a\right) = \frac{\left(\sqrt{2\sigma}\right)^{\mu+\frac{1}{2}}}{\sqrt{\pi}.\left(2\right)^{\mu-\frac{1}{2}}.\Gamma\left(\mu\right)}\left|I^a\right|^{\mu-\frac{1}{2}}\mathcal{K}_{\mu-\frac{1}{2}}\left(\sqrt{2\sigma}\left|I^a\right|\right). \tag{19}$$

$\mathcal{K}_{\mu-\frac{1}{2}}\left(\sqrt{2\sigma}|I^a|\right)$ denotes Bessel function of the second kind [33].

$$\lim_{I^a\to 0} p_{marginal}\left(I^a\right) = \begin{matrix} \sqrt{\frac{2\sigma}{\pi}}.\frac{\Gamma\left(\mu-\frac{1}{2}\right)}{\Gamma\left(\mu\right)}, \; if \; \mu > \frac{1}{2} \\ \infty, \; otherwise. \end{matrix} \tag{20}$$

The tails of this distribution decrease in $|I^a|^{\mu-1}\exp\left(\frac{\sqrt{2\sigma}}{|I^a|}\right)$. This class of prior follows a normal gamma prior estimate [23], [26]. The priors of the image have been computed using the MAP estimate. The two cases of noise matrix are considered i.e. finite or asymptotic which have been used to establish the properties of noise models. Thus, different conditions have been established under which MAP estimate of I^a works. The Gamma PDF can be written in terms of shape and rate parameterization such that

$$f\left(I^a,\alpha,\beta\right)=\frac{\beta^\alpha(I^a)^{\alpha-1}}{\Gamma(\alpha)}\exp\left(-\beta I^a\right),I^a>0,\alpha\beta>0. \tag{21}$$

α and β are shape and rate parameters respectively. The joint Gamma PDF can be written as

$$f\left(I^a,\mu,\sigma^2,\alpha,\beta\right)=\frac{\beta^\alpha}{\Gamma(\alpha)\sqrt{2\pi}}(\sigma)^{\alpha-\frac{1}{2}}\exp\left(-\frac{\beta}{\sigma}\right)\exp\left(-\frac{(I^a-\mu)^2}{2\sigma^2}\right). \tag{22}$$

Using eq. (9), the posterior estimate is written as

$$p\left(I\mid I^a\right)=\frac{(\sigma)^{\alpha-\frac{1}{2}}.\Gamma(\alpha).\exp\left(-\frac{\beta}{\sigma}\right)\exp\left(-\frac{(I^a-\mu)^2}{2\sigma^2}\right)}{\Gamma(\alpha)\sqrt{2\pi}.(I^a)^{\alpha-1}.\exp\left(-\beta I^a\right)},\quad I^a>0. \tag{23}$$

One of the good estimations for different noise models is maximum likelihood [30], [46]. In this paper the advantages of both priors and likelihood have been utilized. The PDF of Gamma distribution with mean (μ) and variance (σ^2) is given as

$$f_{gamma}\left(I^a\right)=\frac{(I^a)^{\mu-1}}{\left(\sigma^2\right)^\mu\Gamma(\mu)}\exp\left(-\frac{I^a}{\sigma^2}\right)I^a>0. \tag{24}$$

A useful generalization is written as

$$f_{gamma}\left(I^a\right)=\frac{\beta(I^a)^{\beta\mu-1}}{\left(\sigma^2\right)^{\beta\mu}\Gamma(\mu)}\exp\left(-\frac{I^a}{\sigma^2}\right)^\beta I^a>0\ and\ \beta>0. \tag{25}$$

As we observe that Gamma distribution is a specialized case when $\beta=1$.

2) MAXIMIZATION OF LIKELIHOOD ESTIMATION

The Gamma distribution can be estimated by computing the likelihood equations. Multiplicative noise follows Gamma distribution which is represented as a function of (μ,σ^2,β) [3]. We will calculate the generalized Gamma distribution with β unknown. The log-likelihood function is based on I^a_{ij} is

$$\mathbb{L}_{gamma}\left(\mu,\sigma^2,\beta\right)=\ln\beta-\beta\mu\ln\sigma^2-\ln\Gamma(\mu)+\frac{1}{MN}\sum_{i=0}^{M-1}\sum_{j=1}^{N-1}\left[(\beta\mu-1)\ln I^a_{ij}-\left(\frac{I^a_{ij}}{\sigma^2}\right)^\beta\right]. \tag{26}$$

The likelihood of equation is obtained by taking partial derivatives w.r.t. $\mu\sigma^2$ and β

$$0=-\frac{d\ln\Gamma(\mu)}{dI^a}-\beta\ln\mu+\frac{\beta}{MN}\sum_{i=0}^{M-1}\sum_{j=1}^{N-1}\ln I^a_{ij}, \tag{27a}$$

$$0=-\mu+\frac{1}{MN}\sum_{i=0}^{M-1}\sum_{j=1}^{N-1}\left(\frac{I^a_{ij}}{\mu}\right)^\beta, \tag{27b}$$

$$0=\frac{1}{\beta}+\frac{k}{MN}\sum_{i=0}^{M-1}\sum_{j=1}^{N-1}\ln\frac{I^a_{ij}}{\mu}-\frac{1}{MN}\sum_{i=0}^{M-1}\sum_{j=1}^{N-1}\left(\frac{I^a_{ij}}{\sigma^2}\right)^\beta\ln\left(\frac{I^a_{ij}}{\sigma^2}\right). \tag{27c}$$

The maximum likelihood estimation is defined by solving eq. (27c). In eq. (27b), σ^2 can be expressed as a function of μ and β

$$\sigma^2(\mu,\beta)=\left(\sum_{i=0}^{M-1}\sum_{j=1}^{N-1}\frac{\left(I^a_{ij}\right)^\beta}{MN\mu}\right)^{\frac{1}{\beta}}. \tag{28}$$

Substitute eq. (28) in eq. (27c), (29), as shown at the bottom of the next page.

It is known that for Gamma distribution $\beta=1$. So, we can represent maximum likelihood estimate for μ and σ^2 as (30a) and (30b), shown at the bottom of the next page.

Eqs. (30a) and (30b) represent a log-likelihood estimation of generalized Gamma distribution.

C. POISSON NOISE DISTRIBUTION MODEL: CASE 3

The Poisson noise distribution follows a mixed noise model where noise is both additive and multiplicative [47], [48]. Assume that for image I^a the Poisson exponential distribution with mean (μ) and variance $\left(\sigma^2\right)$ is written as

$$f\left(I^a;\mu,\sigma^2\right)=\frac{\mu\sigma^2e^{-\sigma^2I^a-\mu\left(\exp\left(-\sigma^2I^2\right)\right)}}{1-e^\mu}. \tag{31}$$

This distribution converges to an exponential distribution with parameters mean and variance [49]. If PDF decreases then $0<\mu<1$ otherwise $\mu\geq1$.

1) PRIOR AND POISSON NOISE DISTRIBUTION

For Poisson noise distribution we estimate the specification of the prior distribution for the parameters μ and σ^2. The corresponding conjugate prior to Poisson distribution retains the shape Gamma distribution. We use Jeffrey's prior [48], [49] for σ^2 and Gamma prior $\mathrm{g}(\cdot)$ for given μ, which can be written as

$$\mathrm{g}(\mu)\propto\mu^{b_1-1}\exp(-b_2\mu), \tag{32a}$$

$$\mathrm{g}\left(\sigma^2\mid\mu\right)\propto\frac{1}{\sigma^2}. \tag{32b}$$

Now the joint prior for μ and σ^2 is given as

$$\mathrm{g}\left(\mu,\sigma^2\right)\propto\frac{\mu^{b_1-1}}{\sigma^2}\exp(-b_2\mu)\,b_1>0,b_2>0. \tag{33}$$

$b_1 b_2$ are hyper-parameters. Under independent and identically distributed sampling as the exponents grow then the eq. (33) retains the power of μ. This suggests that to obtain the conjugate prior for μ we use a distribution that is a product of powers of μ and $(1-\mu)$ which is normalized as b_1 and b_2 such that $b_1 > -1$ and $b_2 > -1$. This choice of prior distribution can be justified when information about μ and σ^2 is very less. A flat prior distribution is a result of large prior variance while the peaked prior is a result of the small prior variance. However, b_1 and b_2 can be taken as zero, when information about mean and variance is very less.

2) MAXIMIZATION OF LIKELIHOOD ESTIMATION

The likelihood function [50] for the Poisson distribution case can be written as

$$\mathbb{L}_{poisson}\left(\mu,\sigma^2|I^a\right) = \exp\left\{MN\log\left(\mu\sigma^2\right) -\sigma^2\sum\nolimits_{\forall i,j} I_{ij}^a - \mu\sum\nolimits_{\forall i,j} e^{-\sigma^2 I_{ij}^a} - MN\log\left(1-e^{\mu}\right)\right\}. \tag{34}$$

The log likelihood of eq. (34) is

$$\log\left(\mathbb{L}_{poisson}\right) = MN\log\left(\mu\sigma^2\right) - \sigma^2\sum\nolimits_{\forall i,j} I_{ij}^a -\mu\sum\nolimits_{\forall i,j} e^{-\sigma^2 I_{ij}^a} - MN\log\left(1-e^{\mu}\right) \tag{35}$$

Differentiating eq. (35) w.r.t. μ and σ^2 we get two implicit equations in mean and variance as

$$\frac{MN}{\mu} - \sum\nolimits_{\forall i,j} e^{\sigma^2 I_{ij}^a} - \frac{MNe^{-\mu}}{1-e^{-\mu}} = 0, \tag{36a}$$

$$\frac{MN}{\sigma^2} - \sum\nolimits_{\forall i,j} I_{ij}^a + \mu\sum\nolimits_{\forall i,j} I_{ij}^a e^{-\sigma^2 I_{ij}^a} = 0. \tag{36b}$$

After combining the likelihood function from eq. (34) and prior from eq. (33), the joint posterior distribution for μ and σ^2 is computed. The density functions are given as

$$p\left(\mu,\sigma^2|I^a\right) \propto \mathbb{L}_{poisson}\left(\mu,\sigma^2|I^a\right) g\left(\mu,\sigma^2\right), \tag{37a}$$

$$p\left(\mu,\sigma^2|I^a\right) = c^{-1}\mu^{(M+N+b_1-1)}\sigma^{2^{(M+N-1)}} exp\left\{-\sigma^2\sum\nolimits_{\forall i,j} I_{ij}^a - \mu\left(b_2+\sum\nolimits_{\forall i,j} e^{-\sigma^2 I_{ij}^a}\right)\right\}. \tag{37b}$$

Here

$$c = \int_0^\infty \int_0^\infty \mu^{(M+N+b_1-1)}\sigma^{2^{(M+N-1)}} exp\left\{-\sigma^2\sum_{\forall i,j} I_{ij}^a - \mu\left(b_2+\sum_{\forall i,j} e^{-\sigma^2 I_{ij}^a}\right)\right\} d\mu d\sigma^2.$$

By considering the fully conditional distortion, the samples from the posterior distribution are simulated using μ and σ^2 such that

$$p\left(\mu|\sigma^2,I^a\right) \propto \mu^{M+N+b_1-1}\exp\left(-\mu\left(b_2+\sum_{\forall i,j} e^{-\sigma^2 I_{ij}^a}\right) -MN.\log\left(1-e^{-\mu}\right)\right), \tag{38a}$$

$$p\left(\sigma^2|\mu,I^a\right) \propto \sigma^{2^{(M+N-1)}}\exp\left(-\sigma^2\sum_{\forall i,j} I_{ij}^a - \mu\sum_{\forall i,j} e^{-\sigma^2 I_{ij}^a}\right). \tag{38b}$$

Eq. (36a) and eq. (36b) gives likelihood maximized at mean and variance i.e. this computation yields the estimates $\hat{\mu}$ and $\widehat{\sigma^2}$

D. WAVELET TRANSFORMATION COEFFICIENTS

We assume that the individual image pixels are independent. The conditional likelihood of noisy image (I^a) w.r.t. noise-free image (I) is proportional to the sum of squared norm [35] and it can be written as

$$p\left(I^a|I\right) \propto \exp\left(-\frac{\|I^a - I\|_2^2}{\sigma^2}\right). \tag{39}$$

The reconstruction of noisefree image aims to maximize the likelihood equation w.r.t. bivariate conjugate priors of image i.e. μ and σ^2. The equivalent sum of the squared norm in eq. (39) has to be minimized. $\|I^a - I\|_2^2$ represents the sum

$$\mu(\beta) = \frac{\sum_{i=0}^{M-1}\sum_{j=1}^{N-1}\left(I_{ij}^a\right)^\beta}{\beta\sum_{i=0}^{M-1}\sum_{j=1}^{N-1}\left(I_{ij}^a\right)^\beta.\ln I_{ij}^a - \beta\sum_{i=0}^{M-1}\sum_{j=1}^{N-1}\ln I_{ij}^a.\sum_{i=1}^{M-1}\sum_{j=0}^{N-1}\left(I_{ij}^a\right)^\beta} \tag{29}$$

$$\hat{\mu} = \frac{\sum_{i=0}^{M-1}\sum_{j=1}^{N-1} I_{ij}^a}{\beta\sum_{i=0}^{M-1}\sum_{j=1}^{N-1} I_{ij}^a.\ln I_{ij}^a - \sum_{i=0}^{M-1}\sum_{j=1}^{N-1}\ln I_{ij}^a.\sum_{i=1}^{M-1}\sum_{j=0}^{N-1} I_{ij}^a}, \tag{30a}$$

$$\widehat{\sigma^2} = \frac{1}{MN\sum_{i=0}^{M-1}\sum_{j=1}^{N-1} I_{ij}^a.\ln I_{ij}^a - \sum_{i=0}^{M-1}\sum_{j=1}^{N-1}\ln I_{ij}^a.\sum_{i=1}^{M-1}\sum_{j=0}^{N-1} I_{ij}^a} \tag{30b}$$

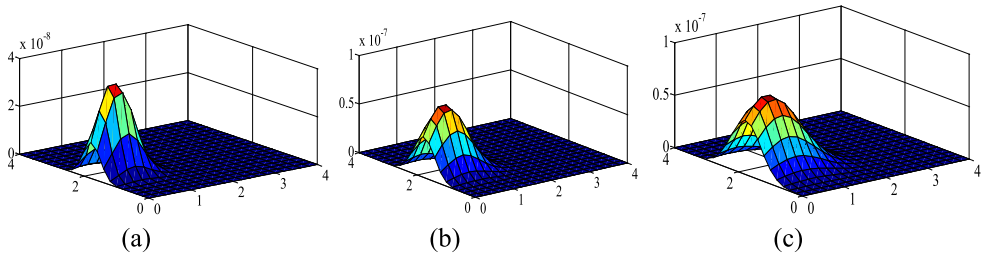

FIGURE 2. Surface plots of proposed methods for image prior density function (a) image size 128 × 128 (b) image size 512 × 512 (c) image size 1024 × 1024.

of squared norm over image pixel space (ij) such that

$$\left\|I^a - I\right\|_2^2 \cong \frac{1}{MN}\sum\nolimits_{\forall i,j}\left\|I_{ij}^a - I_{ij}\right\|_2^2. \tag{40}$$

Since the image priors are less susceptible to variations in pixel intensity because the likelihood estimation improves robustness and reduces bias before the final reconstruction of the noisefree image. In this paper, we opt to use a transformation to represent the image pixels using wavelet coefficients. The procedure to generate high and low frequency wavelet coefficients are detailed in [36]. Let us assume that high frequency and low frequency wavelet coefficients are represented as $\hbar_{ij}$ and ℓ_{ij} respectively. Once the transformation coefficients are estimated we can express the sum of squared norm as

$$\left\|I_{ij}^a - I_{ij}\right\|_2^2 \approx \frac{1}{MN}\sum\nolimits_{\forall i,j}\left\|\hbar_{ij} - \ell_{ij}\right\|_2^2. \tag{41}$$

$\hbar_{ij}$ and ℓ_{ij} are computed from wavelet transformation of the image as $\mathcal{W}^T I_{ij}^a$, where $\mathcal{W}^T$ represents wavelet transformation [45]. The high and low frequency coefficients are computed using wavelet transform and these pixels are identified as aggregate pixels vectors, $\mathcal{N}_{ij}$

E. MINIMIZATION OF NOISY PIXELS

In eq. (40) and eq. (41) the sum of squared norm and noisefree likelihood membership is further optimized using by minimization of $\mathcal{N}_{ij}$. Therefore, we use the minimization problem for noisefree image reconstruction. The transformed pixel vector can be represented using the minimization equation [45] as

$$\mathcal{N}_{ij} = \frac{1}{\sigma^2}\left\|\hbar_{ij} - \ell_{ij}\right\|_2^2 + \lambda_1\left(\hbar_{ij} - \mu_{ij}\right)^T\sum_{\forall i,j}^{-1}\left(\hbar_{ij} - \mu_{ij}\right) + \lambda_2\left\|\hbar_{ij}, \ell_{ij}\right\|_*. \tag{42}$$

$\|.\|_*$ is the nuclear norm [51] of matrix $\mathcal{W}^T I_{ij}^a$ with high and low frequency wavelet coefficients. λ_1 and λ_2 are the weights of the likelihood and nuclear norm terms [51]. We can minimize the overall objective function in eq. (42) by minimizing each term independently. To achieve this, we have used a squared F-norm [51]. The $\mathcal{N}_{ij}$ is minimized w.r.t. low frequency coefficients (l_{ij}) such that the overall effect of high frequency coefficient is maximized. The minimization equation becomes

$$\left(\ell_{ij}^*, \mathcal{N}_{ij}^*\right) = \underset{\ell_{ij},\mathcal{N}_{ij}}{\operatorname{argmin}}\frac{1}{\sigma^2}\left\|\hbar_{ij} - l_{ij}\right\|_2^2 + \lambda_1\left(\hbar_{ij} - \mu_{ij}\right)^T\sum_{\forall i,j}^{-1}\left(\hbar_{ij} - \mu_{ij}\right) + \left\|\mathcal{N}_{ij} - \left[\hbar_{ij}, \ell_{ij}\right]\right\|_F^2 + \lambda_2\left\|\mathcal{N}_{ij}\right\|_*. \tag{43}$$

Here, $\left\|\mathcal{N}_{ij} - \left[\hbar_{ij}, \ell_{ij}\right]\right\|_F^2$ represents squared F-norm. $\left(\ell_{ij}^*, \mathcal{N}_{ij}^*\right)$ represents the minimization of $\mathcal{N}_{ij}$ w.r.t. ℓ_{ij} such that $\mathcal{N}_{ij}^*$ denotes noisefree pixel extraction matrix for the selected low frequency coefficient matrix ℓ_{ij}^*. To solve eq. (43) ℓ_{ij} is varied by keeping $\hbar_{ij}$ fixed in $\mathcal{N}_{ij}$. By doing this, the squared F-norm term becomes a quadratic function of ℓ_{ij}. Therefore, the optimization w.r.t. ℓ_{ij} in $\mathcal{N}_{ij}$ can be written as

$$\left(\ell_{ij}^*, \mathcal{N}_{ij}^*\right) = \underset{\ell_{ij},\mathcal{N}_{ij}}{\operatorname{argmin}}\frac{1}{\sigma^2}\left\|\hbar_{ij} - \ell_{ij}\right\|_2^2 + \lambda_1\left(\hbar_{ij} - \mu_{ij}\right)^T\sum_{\forall i,j}^{-1}\left(\hbar_{ij} - \mu_{ij}\right) + \frac{\left\|\mathcal{N}_{ij}\left[:, \hbar_{ij}\right] - \ell_{ij}\right\|_2^2}{(MN+1)\,\sigma^2}. \tag{44}$$

$\frac{1}{(MN+1)\sigma^2}$ is Lagrange multiplier [45] which is used to represented the F-norm in form of the squared norm. $\mathcal{N}_{ij}\left[:, \hbar_{ij}\right]$ represents the pixel vector with high frequency coefficients. Since eq. (44) is quadratic therefore, its derivative will give a linear equation as

$$\left(\frac{MN+2}{MN+1} + \lambda, \sigma^2.\sum\nolimits_{\forall i,j}^{-1}\hbar_{ij} - \mu_{ij}\right)$$
$$\ell_{ij}^* = \hbar_{ij} + \lambda_1\sigma^2\sum\nolimits_{\forall i,j}^{-1}\mu_{ij} + \frac{\mathcal{N}_{ij}\left[:, \hbar_{ij}\right]}{MN+1}. \tag{45}$$

F. FINAL IMAGE RECOVERY

The transformation coefficients are estimated and we can recover them as the final denoised image $(\mathcal{F})$ in pixel domain by inverse wavelet transform. It can be represented as

$$\mathcal{F} = \mathcal{W}\left(\left(\ell_{ij}^*, \mathcal{N}_{ij}^*\right)\right), \forall ij. \tag{46}$$

Here, $\mathcal{W}$ is the inverse wavelet transform. To reconstruct the full image, we use the transformation coefficients and

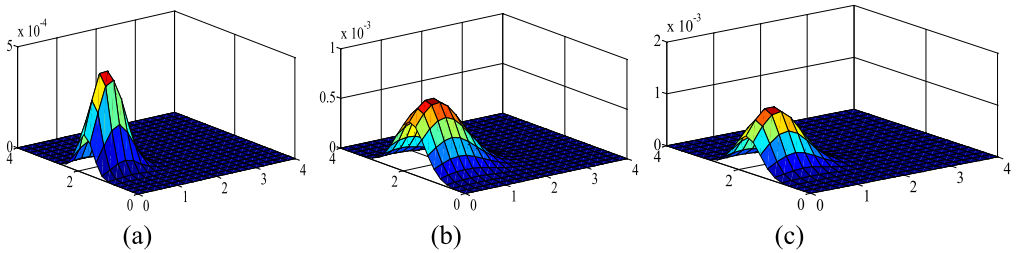

FIGURE 3. Surface plots of proposed method for posterior density function (a) image size 128 × 128 (b) image size 512 × 512 (c) image size 1024 × 1024.

transformed noisefree pixels only. The noisefree pixel extraction matrix is represented as $\mathcal{N}_{ij}^{*}$ such that $\mathcal{F} = \sum_{\forall i,j} \mathcal{N}_{ij}^{*} I_{ij}$. The optimal solution to this minimization problem is

$$\mathcal{F} = \underset{\ell_{ij}}{\operatorname{argmin}}\, \lambda_0 \left\| I^a - \ell_{ij} I^a \right\|_2^2 + \sum\nolimits_{\forall i,j} \left\| \mathcal{N}_{ij}^{*} I - I^a \right\|_2^2. \tag{47}$$

λ_0 is a positive constant. The leastsquare solution of eq. (47) is

$$\mathcal{F} = \left(\lambda_0 I + \sum\nolimits_{\forall i,j} \mathcal{N}_{ij}^{*} I \right)^{-1} \left(\lambda_0 I^a + \sum\nolimits_{\forall i,j} \mathcal{N}_{ij}^{*} I^a \right). \tag{48}$$

Eq. (48) represents the final denoised image.

G. PROPOSED ALGORITHM

The algorithm used in the proposed method has been defined in Algorithm 1.

Algorithm 1 Proposed Algorithm

1) Input: Original image $\boldsymbol{I}$ of size $\boldsymbol{M} \times \boldsymbol{N}$.
2) Introduce Gaussian, Gamma or Poisson noise which yields noisy image $(\boldsymbol{I^a})$.
3) Compute overall discrete gradient from horizontal and vertical discrete gradient.
4) Evaluate probability of noisy image w.r.t mean and variance of prior.
5) Evaluate absolute values of probability of noisy image w.r.t. discrete gradient in case of priors.
6) Evaluate the conditional probability of noisy image w.r.t. noise-free image using MAP estimate.
7) Substitute the values of probabilities in step 6 in terms of the gradient.
8) The log-likelihood estimate is computed for noisy images for Gaussian, Gamma, and Poisson cases.
9) Maximize the equation from step 8 w.r.t. mean and variance to calculate maxima point.
10) High frequency and low frequency wavelet coefficients are represented as $\boldsymbol{\hbar_{ij}}$ and $\boldsymbol{\ell_{ij}}$ respectively. Once the transformation coefficients are estimated we can express them as the sum of squared norm.
11) The sum of squared norm and noise-free likelihood membership is optimized using by minimization of aggregate pixels vector $(\boldsymbol{\mathcal{N}_{ij}})$
12) $\boldsymbol{\mathcal{N}_{ij}}$ is minimized w.r.t. low frequency coefficients $(\boldsymbol{\ell_{ij}})$ and the overall effect of high frequency coefficient is maximized.
13) To reconstruct the full image, we use the transformation coefficients and transformed noise-free pixels only. Finally, the optimal solution of the minimization problem yields noise-free output image.
14) Output: $\boldsymbol{\mathcal{F} = \underset{\ell_{ij}}{\operatorname{argmin}}\, \lambda_0 \left\| I^a - \ell_{ij} I^a \right\|_{\mathbf{F}}^2 + \sum_{\forall i,j} \left\| \mathcal{N}_{ij}^{*} I - I^a \right\|_{\mathbf{F}}^2}$ /∗ Final noise free image ∗/

IV. PERFORMANCE MEASURES

This paper presents a comparison of the proposed method with the conventional algorithms to analyze the performance of the proposed method. It is observed that the expected estimation of the parameters has been successfully recovered using the posterior distribution. We have used mean and variance as the parameter of interest to simulate the statistical estimation using the posterior distribution and computed its bias. Eqs. (12), (23), and (37b) present the estimation of the posterior distribution for different noise models. It is assumed that this estimation is based on the image space. This paper considers different image sizes as 1024×1024.512×512 and 128×128. It is observed that when the image size is small the distribution of posterior estimate is not uniformly distributed. On the other hand, when the image size is large then the distribution of posterior estimate is uniformly distributed which is shown in the surface plots. Figures 2–4 present the surface plots for prior, posterior and likelihood functions respectively. The posterior estimation has been analyzed w.r.t. statistical parameters in terms of bias (B). It is also observed in the surface plots in Figures 2–4 that when the variance is small then the prior estimate truncates the long tails of the likelihood function.

In this paper we have considered different image sizes and plotted the normal prior, log-likelihood and posterior in Figures 2–4 respectively. We have considered the Gaussian distributed noise samples for these plots. It is observed that for all the three image sizes the likelihood function is uniformly distributed about the center for the parameters under consideration i.e. mean and variance. It is observed that

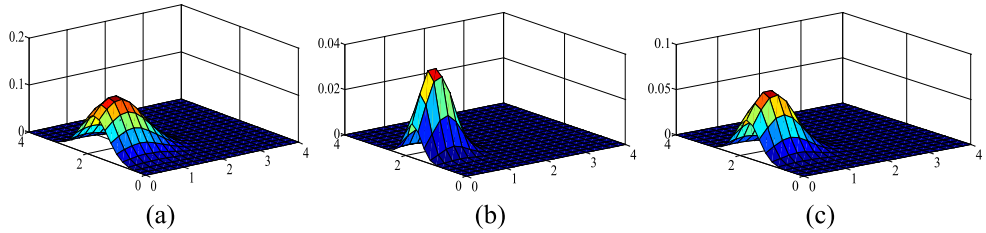

FIGURE 4. Surface plots of proposed method for likelihood function (a) image size 128 × 128 (b) image size 512 × 512 (c) image size 1024 × 1024.

TABLE 1. Values of various performance parameters using proposed algorithm for Gaussian 20dB noise case.

Gaussian (20dB)	PSNR	Q	E	Time	$\mathbb{C}$	SSIM
Maximum Likelihood estimate	22.58	0.31	4.33	3.14	0.31	9.45
Low frequency coefficient transformation	32.76	0.45	6.28	4.55	0.45	13.71
Transformed aggregate image pixels	47.52	0.65	9.11	6.61	0.65	19.89
Noise free pixel-wise extraction of image	60.89	0.83	11.67	8.46	0.84	25.48
Optimized image	67.32	0.92	12.90	9.36	0.93	28.17
Final denoised image	70.18	0.95	14.21	9.78	0.95	28.98

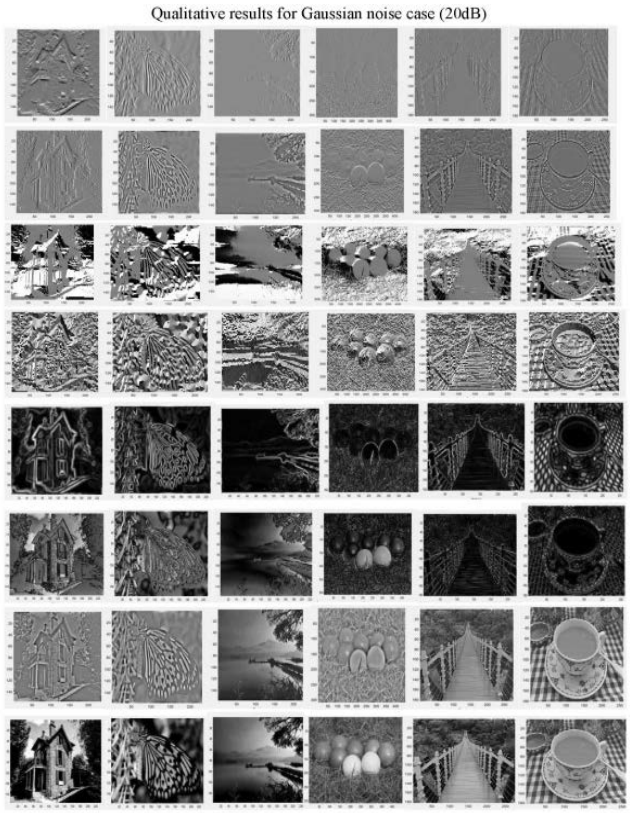

FIGURE 5. The proposed method based qualitative image restoration results for 6 grayscale images (512 × 512) for Gaussian 20dB noise case (Row 1: High frequency coefficients based restoration; Row2: Low frequency coefficients based restoration; Row 3: Aggregate transformation; Row4: Log-Likelihood based restoration; Row5: Minimized $\mathcal{N}_{ij}$ w.r.t high frequency; Row 6: Minimized $\mathcal{N}_{ij}$ w.r.t low frequency; Row7: Optimized image; Row8: Final denoised image).

posterior distribution resembles prior distribution for smaller image size which is well illustrated from eqs. (12), (23), and (37b). When the image size increases the log-likelihood distribution becomes more peaked and the area surrounding the peak is zero. It is observed that the peak of log-likelihood distribution increases when the prior has a small variance, and vice versa. Generally, these estimates are less affected by prior; but, in practical applications, there is a critical sample size for which prior can influence the estimation. It is observed that exponential posterior distribution is estimated using mean and variance. The bias value becomes small when the image size is large and vice versa. Thus, it is concluded that the root men square error can be reduced for a large range of image space because in that case the bias value also reduces. The smaller bias value depicts better efficiency of estimate. The bias value w.r.t. mean and variance is mathematically written as

$$\mathcal{B}_{mean} = \left\| \hat{\mu} - \mu \right\| \tag{49a}$$

$$\mathcal{B}_{variance} = \left\| \widehat{\sigma^2} - \sigma^2 \right\|. \tag{49b}$$

$\hat{\mu}$ is log-likelihood of mean estimate and μ is a true mean estimate. $\widehat{\sigma^2}$ is log-likelihood of variance estimate and σ^2 true mean estimate. $\|.\|$ is absolute value norm. The maximum likelihood estimate for mean and variance is sample mean and variance of data respectively. The larger variance value causes mean square error to increase.

Entropy (E) is the information content of the image and it is represented as $E = -\sum_{i=0}^{L-1} D_i log_2 D_i$ Here, L is the total of grey levels, $D_i = \{D_0, D_1, \ldots, D_{L-1}\}$ is the probability distribution of each level. Root mean square error (RMSE) corresponds to noisy pixels in F and I^a. RMSE value will increase when the noisy pixels increase between these two images. Mathematically

$$RMSE = \sqrt{\frac{1}{MN} \sum_{i=0}^{M-1} \sum_{j=0}^{N-1} (\mathcal{F}_{ij} - I_{ij}^a)^2}. \tag{50}$$

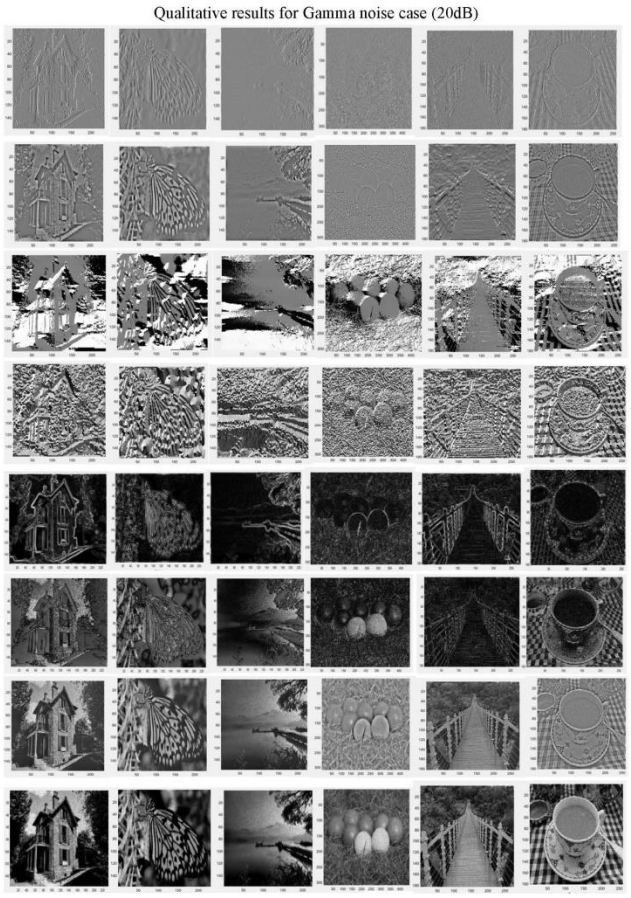

FIGURE 6. The proposed method based qualitative image restoration results for 6 grayscale images (512 × 512) for Gamma 20dB noise case (Row 1: High frequency coefficients based restoration; Row2: Low frequency coefficients based restoration; Row 3: Aggregate transformation; Row4: Log-Likelihood based restoration; Row5: Minimized $\mathcal{N}_{ij}$ w.r.t high frequency; Row 6: Minimized $\mathcal{N}_{ij}$ w.r.t low frequency; Row7: Optimized image; Row8: Final denoised image).

TABLE 2. Values of various performance parameters using proposed algorithm for Gamma 20dB noise case.

Gamma (20dB)	PSNR	Q	E	Time	$\mathbb{C}$	SSIM
Maximum Likelihood estimate	20.00	0.29	3.83	3.11	0.29	6.87
Low frequency coefficient transformation	32.85	0.47	6.29	5.10	0.48	11.29
Transformed aggregate image pixels	42.09	0.61	8.07	6.54	0.62	14.46
Noise free pixel-wise extraction of image	53.93	0.78	10.34	8.37	0.80	18.53
Optimized image	58.99	0.85	11.31	9.16	0.87	20.27
Final denoised image	62.15	0.89	11.75	9.58	0.91	22.91

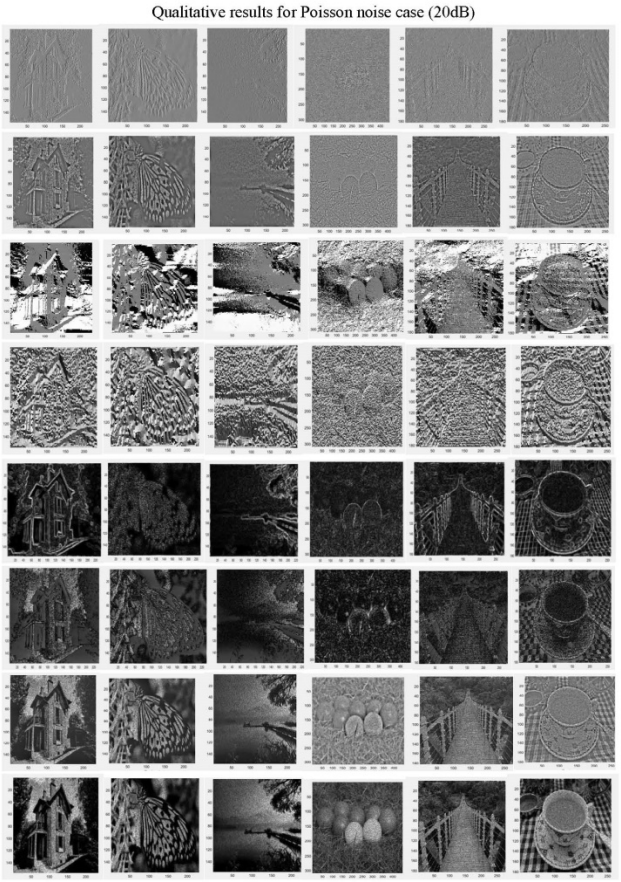

FIGURE 7. The proposed method based qualitative image restoration results for 6 grayscale images (512 × 512) for Poisson 20dB noise case (Row 1: High frequency coefficients based restoration; Row2: Low frequency coefficients based restoration; Row 3: Aggregate transformation; Row4: Log-Likelihood based restoration; Row5: Minimized $\mathcal{N}_{ij}$ w.r.t high frequency; Row 6: Minimized $\mathcal{N}_{ij}$ w.r.t low frequency; Row7: Optimized image; Row8: Final denoised image).

TABLE 3. Values of various performance parameters using proposed algorithm for Poisson 20dB noise case.

Poisson (20dB)	PSNR	Q	E	Time	$\mathbb{C}$	SSIM
Maximum Likelihood estimate	20.33	0.28	3.70	3.00	0.28	6.64
Low frequency coefficient transformation	28.74	0.46	6.08	4.93	0.47	10.91
Transformed aggregate image pixels	50.67	0.59	7.79	6.32	0.60	13.98
Noise free pixel-wise extraction of image	62.11	0.75	9.99	8.09	0.77	17.91
Optimized image	67.00	0.82	10.92	8.85	0.84	19.59
Final denoised image	78.28	0.95	14.88	10.77	0.97	20.28

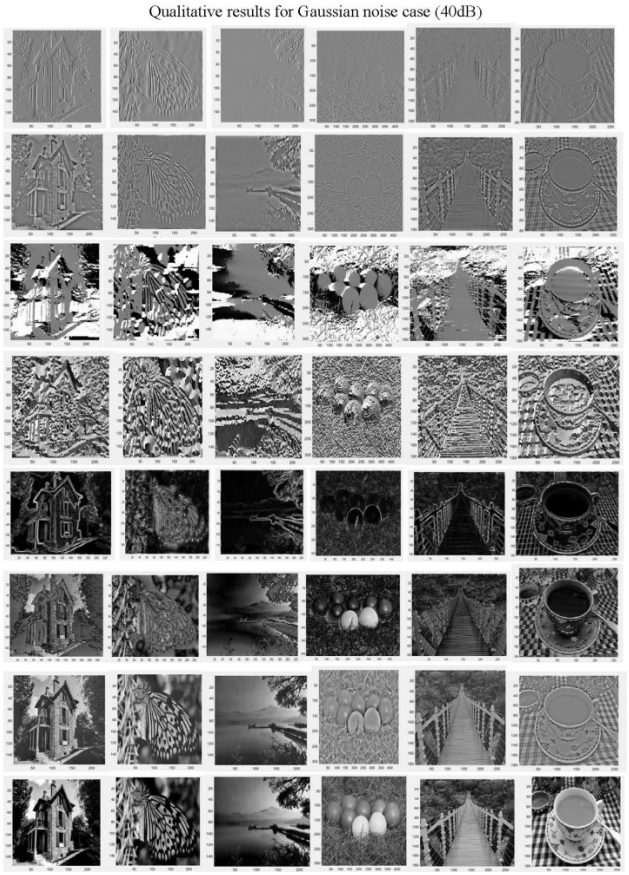

FIGURE 8. The proposed method based qualitative image restoration results for 6 grayscale images (512 × 512) for Gaussian 40dB noise case (Row 1: High frequency coefficients based restoration; Row2: Low frequency coefficients based restoration; Row 3: Aggregate transformation; Row4: Log-Likelihood based restoration; Row5: Minimized $\mathcal{N}_{ij}$ w.r.t high frequency; Row 6: Minimized $\mathcal{N}_{ij}$ w.r.t low frequency; Row7: Optimized image; Row8: Final denoised image).

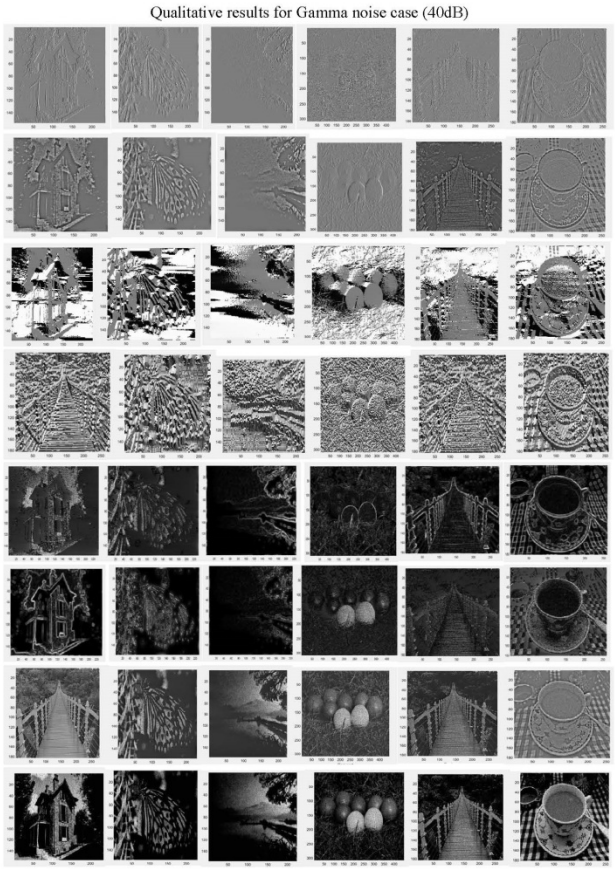

FIGURE 9. The proposed method based qualitative image restoration results for 6 grayscale images (512 × 512) for Gamma 40dB noise case (Row 1: High frequency coefficients based restoration; Row2: Low frequency coefficients based restoration; Row 3: Aggregate transformation; Row4: Log-Likelihood based restoration; Row5: Minimized $\mathcal{N}_{ij}$ w.r.t high frequency; Row 6: Minimized $\mathcal{N}_{ij}$ w.r.t low frequency; Row7: Optimized image; Row8: Final denoised image).

TABLE 4. Values of various performance parameters using proposed algorithm for Gaussian 40dB noise case.

Gaussian (40dB)	PSNR	Q	E	Time	$\mathbb{C}$	SSIM
Maximum Likelihood estimate	16.84	0.25	2.03	2.63	0.24	6.11
Low frequency coefficient transformation	27.65	0.42	3.33	4.32	0.40	10.03
Transformed aggregate image pixels	35.43	0.54	4.26	5.54	0.51	12.85
Noise free pixel-wise extraction of image	51.39	0.78	6.18	8.04	0.75	18.64
Optimized image	58.67	0.89	7.06	9.17	0.85	21.28
Final denoised image	64.08	0.97	7.71	10.02	0.93	23.24

TABLE 5. Values of various performance parameters using proposed algorithm for Gamma 40dB noise case.

Gamma (40dB)	PSNR	Q	E	Time	$\mathbb{C}$	SSIM
Maximum Likelihood estimate	14.88	0.23	1.79	2.33	0.22	5.39
Low frequency coefficient transformation	24.43	0.37	2.94	3.82	0.35	8.86
Transformed aggregate image pixels	31.30	0.47	3.77	4.89	0.45	11.35
Noise free pixel-wise extraction of image	45.40	0.69	5.46	7.10	0.66	16.47
Optimized image	51.79	0.79	7.04	9.02	0.75	15.99
Final denoised image	56.57	0.86	7.69	9.85	0.82	17.46

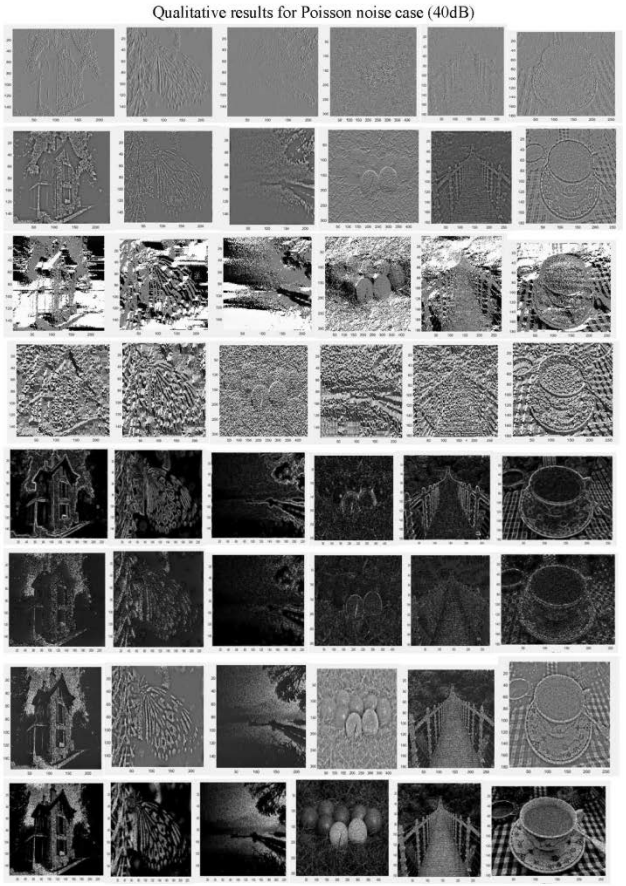

FIGURE 10. The proposed method based qualitative image restoration results for 6 grayscale images (512 × 512) for Poisson 40dB noise case (Row 1: High frequency coefficients based restoration; Row2: Low frequency coefficients based restoration; Row 3: Aggregate transformation; Row4: Log-Likelihood based restoration; Row5: Minimized $\mathcal{N}_{ij}$ w.r.t high frequency; Row 6: Minimized $\mathcal{N}_{ij}$ w.r.t low frequency; Row7: Optimized image; Row8: Final denoised image).

The average correlation $\mathbb{C}$ can be expressed as

$$\mathbb{C} = \frac{\mathcal{F}_{ij}.I^a_{ij}}{\sqrt{\sum_{i=0}^{M-1}\sum_{j=0}^{N-1}(I^2_{ij}+I^{a^2}_{ij})}}. \tag{51}$$

The average correlation metric provides a quantitative measure of the degree of correlation. The image quality improves when $\mathbb{C}$ is closer to 1. Another performance metric is, Image quality Index ($\mathcal{Q}$) which is used to measure image distortion in terms of three factors i.e. loss of correlation, luminance distortion and constant distortion. We considered two images i.e. noisy (I^a) and denoised image ($\mathcal{F}$). The notation d represents the degree of correlation. The image quality index is calculated as a product of three components. It is written as

$$\mathcal{Q} = \frac{d(\mathcal{F}, I^a)}{d(\mathcal{F})\,d(I^a)}\,\frac{2\bar{d}(\mathcal{F})\,\bar{d}(I^a)}{\bar{d}(\mathcal{F})^2+\bar{d}(I^a)^2}\,\frac{2d(\mathcal{F})\,d(I^a)}{d(\mathcal{F})^2+d(I^a)^2}. \tag{52}$$

$$\bar{d}(\mathcal{F}) = \frac{1}{M\times N}\sum_{i=0}^{M-1}\sum_{j=0}^{N-1}\mathcal{F}_{ij} \tag{53a}$$

TABLE 6. Values of various performance parameters using proposed algorithm for Poisson 40dB noise case.

Poisson (40dB)	PSNR	$\mathcal{Q}$	E	Time	$\mathbb{C}$	SSIM
Maximum Likelihood estimate	18.16	0.23	2.47	2.84	0.25	4.49
Low frequency coefficient transformation	23.27	0.29	3.16	3.64	0.32	5.75
Transformed aggregate image pixels	33.75	0.42	4.59	5.28	0.46	8.34
Noise free pixel-wise extraction of image	43.25	0.54	5.88	6.76	0.59	10.68
Optimized image	47.24	0.59	6.42	7.39	0.64	11.67
Final denoised image	**71.61**	**0.9**	**9.73**	**11.2**	**0.97**	**17.69**

$$\bar{d}(I^a) = \frac{1}{M\times N}\sum_{i=0}^{M-1}\sum_{j=1}^{N-1}I^a_{ij} \tag{53b}$$

$$d(\mathcal{F}I^a) = \frac{1}{M+N-1}\sum_{i=0}^{M-1}\sum_{j=0}^{N-1}\left(\mathcal{F}_{ij}-\bar{d}(I^a)\right)\left(I^a_{ij}-\bar{d}(I^a)\right) \tag{53c}$$

$$d(\mathcal{F})^2 = \frac{1}{M+N-1}\sum_{i=0}^{M-1}\sum_{j=0}^{N-1}\left(\mathcal{F}_{ij}-\bar{d}(I)\right)^2 \tag{53d}$$

$$d(I^a)^2 = \frac{1}{M+N-1}\sum_{i=0}^{M-1}\sum_{j=0}^{N-1}\left(I^a_{ij}-\bar{d}(I^a)\right)^2. \tag{53e}$$

The degree of linear correlation is measured using the first component whose values lie between -1 to 1. The closeness of the mean luminance (or contrast of images) between images $\mathcal{F}_{ij}$ and I^a_{ij} is measured using the second component whose value lies between 0 to 1. The similarity of contrast between images is measured using the third component whose value lies between 0 to 1. The best value of $\mathcal{Q}$ is assumed to be unity.

Peak signal to noise ratio ($PSNR$) is calculated as

$$PSNR = 20log_{10}\left(\frac{L^2}{\frac{1}{MN}\sum_{i=0}^{M-1}\sum_{j=0}^{N-1}(\mathcal{F}_{ij}-I^a_{ij})^2}\right). \tag{54}$$

Here, L is the number of gray levels in the image. A high PSNR value corresponds to a better qualitative image. Structural similarity index measure ($SSIM$) [52], [53] is used for determining the structural similarity between two images as it takes into account the characteristics of the human visual system. The $SSIM$ of the image $\mathcal{F}$ and I_{ij} is given as

$$SSIM = \frac{\sum SSIM(\mathcal{F}_{ij}, I_{ij})}{M\times N}. \tag{55}$$

FIGURE 11. Qualitative results for Gaussian noise at 20dB (512 × 512) (Row 1: Proposed method; Row2: MLE [21]; Row 3: VMAP [22]; Row 4: BHE [28]; Row5: SCA [29]; Row6: BMM [30]; Row7: HBN [31]; Row8: VBA [33] and Row9: ADM [34]).

$SSIM(\mathcal{F}_{ij}, I_{ij})$ is the similarity of the image in the $i \times j$ space $\mathcal{F}_{ij}$ and I_{ij} is given by

$$SSIM\left(\mathcal{F}_{ij}, I_{ij}\right) = \frac{\left(2\mu_{\mathcal{F}_{ij}}\mu_{I_{ij}}\right)\left(2\sigma_{\mathcal{F}_{ij}}\mu_{I_{ij}}\right)}{\left(\mu^2_{\mathcal{F}_{ij}} + \mu^2_{I_{ij}}\right)\left(\sigma^2_{\mathcal{F}_{ij}} + \sigma^2_{I_{ij}}\right)}. \quad (56)$$

$\mu_{F_{ij}}$ and $\mu_{I_{ij}}$ are the local means, $\sigma^2_{F_{ij}}$ and $\sigma^2_{I_{ij}}$ are the variance for images F_{ij} and I_{ij} respectively.

Figures 5–10 represent qualitative results for different stages of the proposed method for 6 grayscale images under different noise cases i.e. Gaussian 20dB, Gamma 20dB, Poisson 20dB, Gaussian 40dB, Gamma 40dB and Poisson 40dB respectively. The different rows of Figures 5–10 indicate the following: Row 1: High frequency coefficients based restoration; Row2: Low frequency coefficients based restoration; Row 3: Aggregate transformation; Row4: Log-Likelihood based restoration; Row5: Minimized $\mathcal{N}_{ij}$ w.r.t high frequency; Row 6: Minimized $\mathcal{N}_{ij}$ w.r.t low frequency; Row7: Optimized image; Row8: Final denoised image.

Tables 1–6 represent values of various performance parameters computed for proposed algorithm for different noise cases i.e. Gaussian 20dB, Gamma 20dB, Poisson 20dB, Gaussian 40dB, Gamma 40dB and Poisson 40dB respectively.

V. RESULTS AND DISCUSSION

This paper presents the performance comparison of the proposed algorithm with some existing parametric estimation-based methods [21], [22], [27]–[30], [33] and [34]. for image denoising. It can be observed that the visual quality of an image is improved using the proposed algorithm. The denoising performance of the proposed method has

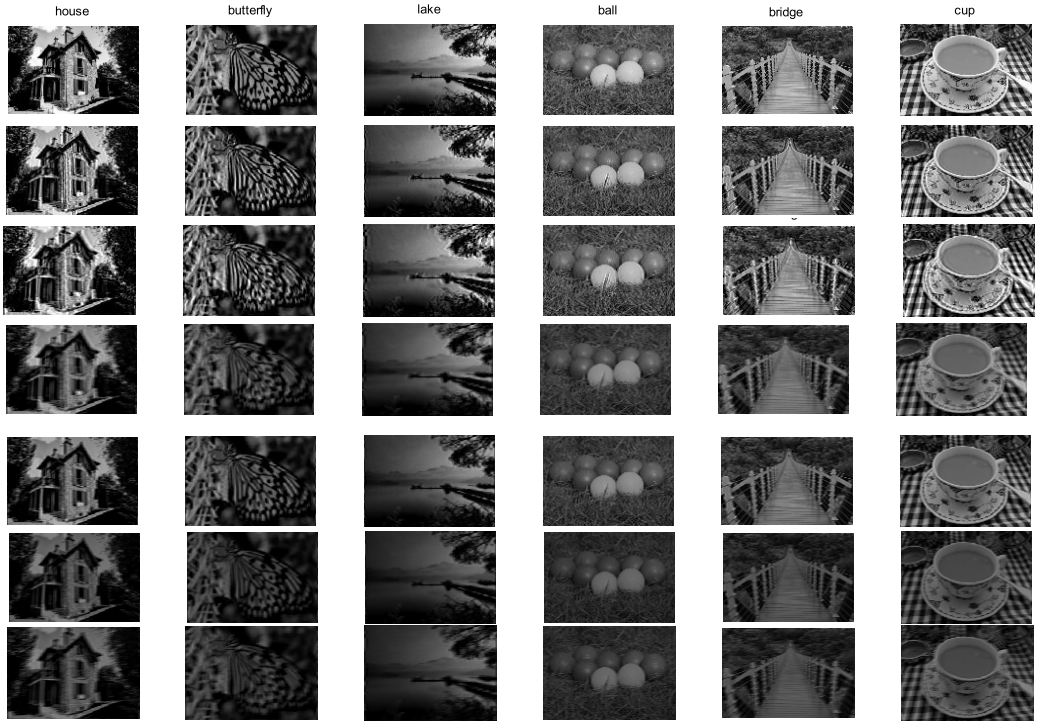

FIGURE 12. Proposed method based qualitative results for 6 images (512 × 512) (Row 1: Original images; Row2: Gaussian noise at 20dB; Row 3: Gamma noise at 20dB; Row4: Poisson noise at 20dB; Row5: Gaussian noise at 40dB; Row 6: Gamma noise at 40dB; Row7: Poisson noise at 40dB).

improved by using Log-likelihood estimation on priors of the image. We performed the experiments on six sets of grayscale images (house, butterfly, lake ball, bridge, and cup). We have considered different noise densities i.e. 20dB and 40dB for our experiments. The qualitative results using various methods [21], [22], [27]–[30], [33], and [34]. have been shown in Figure 11 for Gaussian noise at 20dB. The qualitative results using the proposed method for Gaussian, Gamma, and Poisson-induced noises at 20dB and 40dB are shown in Figure 12. The qualitative results depict that the output image using the proposed method is visually pleasing as compared to other methods.

We have also analyzed one set of the color image from the dataset [54]. Until recently, extensive work has been done related to grayscale images, but the advances in computational power and instrumentation have evolved the research on color images as well [35]. The proposed method can be extended from grayscale to the color images. Thus, the multidimensional capability of the proposed method enables the implementation of more efficient methods in the future as well. The applicability of the proposed method for color images is based on the selection of an appropriate likelihood measure. Figure 13 represents the proposed method based qualitative image restoration results for a color image. The different rows of Figure 13 indicate the following: Row 1: High frequency coefficients based restoration; Row2: Low frequency coefficients based restoration; Row 3: Aggregate transformation; Row4: Log-Likelihood based restoration; Row5: Minimized $\mathcal{N}_{ij}$ w.r.t high frequency; Row 6: Minimized $\mathcal{N}_{ij}$ w.r.t low frequency; Row7: Optimized image; Row8: Final denoised image.

TABLE 7. Values of reliability and statistical estimation parameters for proposed algorithm.

True Scale value	Statistical Estimate		Reliability		
	$\widehat{\mu}$	$\widehat{\sigma^2}$	$\mathcal{B}_{mean}$	$\mathcal{B}_{variance}$	RMSE
Noise Level=20dB					
Gaussian					
1024x1024	106.69	280.45	6.41	33.31	37.35
512x512	111.89	293.80	14.04	26.24	38.25
128x128	116.94	288.84	22.21	23.01	40.35
Gamma					
1024x1024	135.32	286.62	38.36	29.48	49.05
512x512	127.81	293.63	33.11	22.00	39.31
128x128	120.87	289.96	23.69	21.40	32.15
Poisson					
1024x1024	134.34	259.95	42.40	22.04	47.14
512x512	129.26	279.05	36.64	18.61	41.08
128x128	123.83	284.29	29.68	18.55	34.91
Noise Level=40dB					
Gaussian					
1024x1024	109.44	287.68	6.57	34.17	38.31
512x512	114.78	301.37	14.40	26.92	39.24
128x128	119.95	296.28	22.78	23.60	41.39
Gamma					
1024x1024	141.60	299.91	40.14	30.85	51.32
512x512	133.74	307.25	34.65	23.02	41.13
128x128	126.48	303.41	24.78	22.40	33.64
Poisson					
1024x1024	140.57	272.01	44.37	23.06	49.33
512x512	135.26	292.00	38.34	19.48	42.98
128x128	129.57	297.47	31.05	19.40	36.53

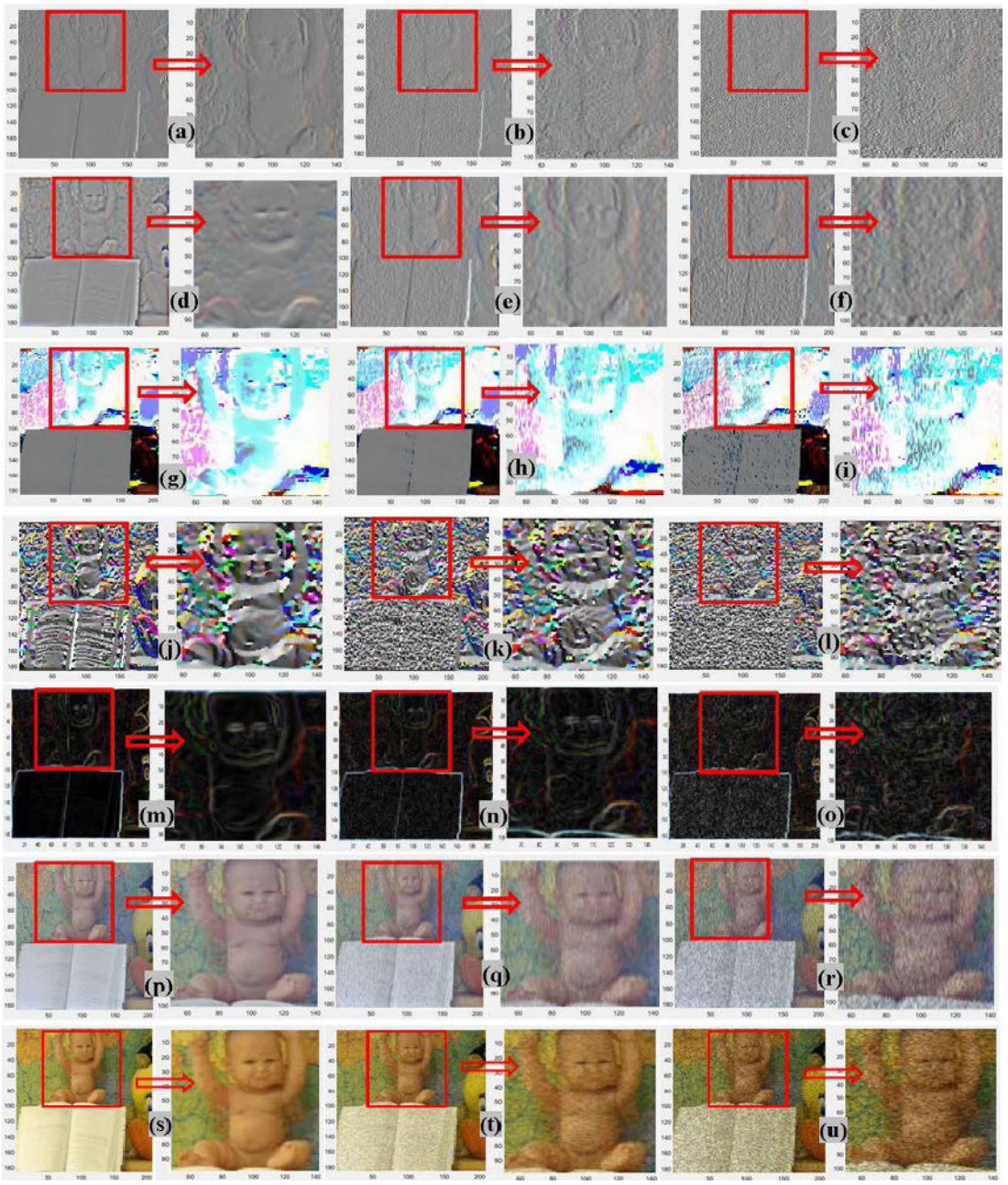

FIGURE 13. The proposed method based qualitative image restoration results for color image (512 × 512) (Col 1,2: Gaussian induced noise (40dB); Col 3,4: Gaussian induced noise (40dB); Col 5,6: Poisson induced noise (40dB)); (Row 1: High frequency coefficients based restoration; Row2: Low frequency coefficients based restoration; Row 3: Aggregate transformation; Row4: Log-Likelihood based restoration; Row5: Minimized $\mathcal{N}_{ij}$ w.r.t high frequency; Row 6: Minimized $\mathcal{N}_{ij}$ w.r.t low frequency; Row7: Optimized image; Row8: Final denoised image).

In this paper, we have quantitatively analyzed the performance of all the algorithms in terms of performance measures such as RMSE, PSNR, Quality Index, Entropy, Correlation coefficient, SSIM. These performance measures consider average pixel intensity under different noise levels i.e. $20dB$ and $40dB$. The input image has been introduced to Gaussian, Gamma and Poisson noise by using a pseudorandom noise generator. We generate a noised image by scaling the ideal intensity image I^a by a factor $\mathtt{n}$ such that the final image becomes $(\mathtt{n}.I^a)$.The scale factor $\mathtt{n}$ is used to control the average intensity of the image. The value of $\mathtt{n}$ is small under low light conditions. We have chosen its value as twice the average pixel intensity value of $E(\mathtt{n}I^a)$. In our experiments, we have chosen average pixel intensity value of $E(\mathtt{n}I^a)$ as 0.05, 0.1, 0.5, 1 and 1.5. We have used PSNR and SSIM to benchmark denoising performance as shown in tabulation results.

TABLE 8. Performance metric based comparison under Gaussian noise distribution for an average of image sets.

	MLE [21]	VMAP [22]	BHE [27]	SCA [28]	BMM [29]	HBN [30]	VBA [33]	ADM [34]	Proposed
Noise level=20dB									
PSNR	53.55	61.22	66.41	63.75	66.70	68.15	65.60	57.10	**69.13**
Q	0.79	0.80	0.91	0.83	0.91	0.85	0.89	0.85	**0.94**
E	9.88	9.28	11.08	9.66	10.70	11.53	10.52	10.53	**13.25**
Time	**9.12**	9.19	9.34	10.57	10.59	9.73	9.43	9.37	9.61
$\mathbb{C}$	0.87	0.87	0.96	0.91	0.89	0.90	0.88	0.92	**0.95**
Noise level=40dB									
PSNR	56.36	59.27	61.50	61.72	61.64	62.03	60.62	57.72	**64.08**
Q	0.69	0.70	0.88	0.73	0.81	0.91	0.79	0.71	**0.97**
E	6.58	6.71	7.46	6.98	6.97	6.76	6.86	6.74	**7.71**
Time	**9.36**	9.59	9.74	10.98	10.00	10.14	9.84	9.59	10.02
$\mathbb{C}$	0.78	0.80	0.87	0.84	0.83	0.89	0.81	0.80	**0.93**

TABLE 9. Performance metric based comparison under Gamma noise distribution for an average of image sets.

	MLE [21]	VMAP [22]	BHE [27]	SCA [28]	BMM [29]	HBN [30]	VBA [33]	ADM [34]	Proposed
Noise level=20dB									
PSNR	43.38	49.59	53.79	56.28	58.88	57.04	53.14	50.40	**61.05**
Q	0.64	0.64	0.74	0.73	0.80	0.84	0.73	0.75	**0.88**
E	8.00	7.52	8.97	8.53	9.44	10.18	8.52	9.30	**11.70**
Time	**7.39**	7.44	7.57	9.44	10.47	10.59	7.64	8.59	9.48
$\mathbb{C}$	0.70	0.70	0.78	0.80	0.79	0.78	0.71	0.82	**0.90**
Noise level=40dB									
PSNR	45.65	48.01	49.86	54.48	54.41	54.58	49.10	53.06	**56.57**
Q	0.56	0.56	0.71	0.64	0.71	0.81	0.65	0.65	**0.86**
E	5.33	5.43	6.04	6.17	6.16	6.85	5.55	6.20	**7.69**
Time	**7.58**	7.77	7.89	9.81	10.83	10.95	7.97	8.81	9.85
$\mathbb{C}$	0.63	0.65	0.73	0.74	0.73	0.79	0.66	0.73	**0.82**

TABLE 10. Performance metric based comparison under Poisson noise distribution for an average of image sets.

	MLE [21]	VMAP [22]	BHE [27]	SCA [28]	BMM [29]	HBN [30]	VBA [33]	ADM [34]	Proposed
Noise level=20dB									
PSNR	54.91	62.78	68.09	74.54	71.24	**77.28**	67.26	63.81	77.26
Q	0.81	0.81	0.93	0.82	0.89	**0.98**	0.92	0.85	0.94
E	10.13	9.52	11.36	11.96	10.80	12.89	10.78	11.77	**14.81**
Time	**9.36**	9.42	9.58	10.72	10.69	10.87	9.68	10.88	10.74
$\mathbb{C}$	0.89	0.89	0.98	0.90	0.81	0.91	0.90	0.82	**0.98**
Noise level=20dB									
PSNR	57.79	60.78	63.12	68.88	68.97	**71.63**	62.16	67.16	71.61
Q	0.70	0.71	0.90	0.84	0.81	**0.98**	0.81	0.82	0.90
E	6.75	6.88	7.64	7.79	7.80	8.68	7.04	7.84	**9.73**
Time	**9.60**	9.83	9.98	11.18	11.16	11.33	10.09	11.15	11.20
$\mathbb{C}$	0.80	0.83	0.90	0.89	0.89	0.85	0.83	0.91	**0.97**

In Table 7 the values of statistical estimate and reliability have been calculated by using the proposed method as average values of all image sets. These average values have been computed for different noise densities of 20dB and 40dB under Gaussian, Gamma and Poisson noise. We have considered different image sizes as 1024×1024, 512×512 and 128×128 to compute the values of true values of statistical estimate. The value of the bias parameter is

TABLE 11. a. Variation in PSNR w.r.t. average pixel intensity under different noise distributions for average of image sets at noise level 20dB. b. Variation in PSNR w.r.t. average pixel intensity under different noise distributions for average of image sets at noise level 40dB.

(a)

Average Pixel Intensity	0.05	0.1	0.5	1.0	1.5
Gaussian					
MLE [21]	19.34	20.23	21.69	21.76	25.70
VMAP [22]	20.97	21.60	22.91	24.38	26.19
BHE [27]	24.40	**25.69**	25.33	29.71	29.27
SCA [28]	20.67	21.30	22.59	24.04	25.82
BMM [29]	18.27	18.14	22.47	26.17	28.13
HBN [30]	24.05	25.32	27.93	28.28	29.83
VBA[33]	19.23	17.32	23.85	27.65	27.94
ADM [34]	19.96	20.04	22.18	22.05	24.98
Proposed	**25.42**	25.62	**28.93**	**29.72**	**31.59**
Gamma					
MLE [21]	9.28	9.50	15.88	18.83	23.07
VMAP [22]	10.42	10.84	18.70	21.31	25.36
BHE [27]	13.45	16.40	**20.98**	26.94	26.36
SCA [28]	10.27	10.69	18.44	21.00	25.00
BMM [29]	12.36	12.20	19.11	25.00	27.38
HBN [30]	14.24	16.17	20.61	26.55	26.96
VBA[33]	13.14	12.98	19.99	25.96	27.97
ADM [34]	10.17	9.98	14.94	19.14	23.04
Proposed	**14.44**	**17.90**	**20.98**	**27.68**	**27.97**
Poisson					
MLE [21]	7.99	7.60	14.90	17.47	21.88
VMAP [22]	8.77	10.46	15.88	18.83	23.06
BHE [27]	12.54	12.38	21.77	**25.79**	27.77
SCA [28]	8.64	10.31	15.65	18.56	22.74
BMM [29]	7.64	9.37	**22.49**	25.29	27.67
HBN [30]	12.36	12.20	20.47	25.42	27.38
VBA[33]	8.75	9.80	22.91	25.56	28.98
ADM [34]	7.98	7.95	14.96	18.62	22.05
Proposed	**14.72**	**17.82**	21.25	25.70	**28.44**

(b)

Average Pixel Intensity	0.05	0.1	0.5	1.0	1.5
Gaussian					
MLE [21]	14.38	15.04	16.13	16.18	19.11
VMAP [22]	15.59	16.05	17.04	18.13	19.48
BHE [27]	18.14	19.10	21.07	22.09	23.25
SCA [28]	17.20	17.70	18.80	20.00	21.48
BMM [29]	15.20	15.09	18.70	21.78	23.41
HBN [30]	20.01	21.07	**23.24**	24.37	**25.65**
VBA[33]	14.11	14.01	17.36	20.22	21.73
ADM [34]	16.24	17.00	18.22	18.28	21.59
Proposed	**21.15**	**21.32**	**23.24**	**23.48**	24.62
Gamma					
MLE [21]	6.90	7.06	11.81	14.00	17.15
VMAP [22]	7.75	8.06	13.91	15.85	18.86
BHE [27]	10.74	12.20	15.55	20.03	21.09
SCA [28]	8.55	8.89	15.34	17.48	20.80
BMM [29]	10.29	10.15	15.90	20.81	22.78
HBN [30]	11.85	13.45	17.15	22.10	**23.27**
VBA[33]	9.55	9.42	14.77	19.31	21.15
ADM [34]	7.79	7.98	13.34	15.82	19.38
Proposed	**12.01**	**14.89**	**17.46**	**23.03**	**23.27**
Poisson					
MLE [21]	5.83	5.54	10.86	12.73	15.95
VMAP [22]	6.39	7.63	11.58	13.72	16.81
BHE [27]	9.14	9.02	15.14	18.80	20.25
SCA [28]	7.19	8.58	13.02	15.44	18.92
BMM [29]	6.36	7.79	18.71	21.04	**23.02**
HBN [30]	10.29	10.15	17.04	21.15	22.78
VBA[33]	5.79	7.10	17.03	19.15	20.95
ADM [34]	6.72	6.39	12.51	14.67	18.38
Proposed	**12.25**	**14.83**	**17.69**	**21.39**	22.04

TABLE 12. a. Variation in SSIM w.r.t. average pixel intensity under different noise distributions for average of image sets at noise level 20dB. b. Variation in SSIM w.r.t. average pixel intensity under different noise distributions for average of image sets at noise level 40dB.

(a)

Average Pixel Intensity	0.05	0.1	0.5	1.0	1.5
Gaussian					
MLE [21]	0.39	0.39	0.48	0.45	0.51
VMAP [22]	0.42	0.47	0.49	0.50	0.59
BHE [27]	0.52	0.58	0.70	0.76	0.78
SCA [28]	0.45	0.51	0.53	0.54	0.65
BMM [29]	0.34	0.34	0.50	0.64	0.79
HBN [30]	0.57	0.63	**0.76**	**0.83**	**0.90**
VBA[33]	0.35	0.36	0.48	0.62	0.79
ADM [34]	0.48	0.47	0.57	0.53	0.59
Proposed	**0.64**	**0.75**	**0.76**	0.81	0.85
Gamma					
MLE [21]	0.12	0.13	0.15	0.27	0.50
VMAP [22]	0.14	0.15	0.29	0.49	0.51
BHE [27]	0.31	0.29	0.36	0.66	0.67
SCA [28]	0.15	0.17	0.31	0.53	0.56
BMM [29]	0.15	0.15	0.33	0.54	0.67
HBN [30]	0.34	0.32	0.40	0.72	**0.74**
VBA[33]	0.19	0.19	0.37	0.51	0.67
ADM [34]	0.19	0.21	0.20	0.34	0.57
Proposed	**0.36**	**0.43**	**0.42**	**0.76**	0.73
Poisson					
MLE [21]	0.12	0.12	0.15	0.27	0.43
VMAP [22]	0.12	0.14	0.35	0.38	0.49
BHE [27]	0.14	0.14	0.37	0.56	0.62
SCA [28]	0.13	0.16	0.39	0.41	0.54
BMM [29]	0.11	0.11	0.39	0.54	0.69
HBN [30]	0.15	0.15	0.41	**0.61**	0.68
VBA[33]	0.12	0.15	0.38	0.53	0.66
ADM [34]	0.15	0.16	0.19	0.32	0.51
Proposed	**0.24**	**0.31**	**0.47**	0.47	**0.71**

(b)

Average Pixel Intensity	0.05	0.1	0.5	1.0	1.5
Gaussian					
MLE [21]	0.30	0.30	0.39	0.36	0.42
VMAP [22]	0.32	0.38	0.40	0.41	0.50
BHE [27]	0.43	0.49	0.61	0.67	0.73
SCA [28]	0.36	0.41	0.44	0.45	0.55
BMM [29]	0.24	0.24	0.40	0.54	0.70
HBN [30]	0.47	0.54	**0.67**	**0.74**	**0.81**
VBA[33]	0.24	0.27	0.39	0.52	0.68
ADM [34]	0.34	0.37	0.48	0.42	0.51
Proposed	**0.54**	**0.66**	**0.67**	0.72	0.76
Gamma					
MLE [21]	0.03	0.04	0.06	0.18	0.41
VMAP [22]	0.05	0.06	0.19	0.40	0.42
BHE [27]	0.22	0.20	0.27	0.57	0.58
SCA [28]	0.05	0.07	0.21	0.44	0.46
BMM [29]	0.05	0.06	**0.51**	0.44	0.48
HBN [30]	0.04	**0.08**	0.06	0.50	0.22
VBA[33]	0.07	0.09	0.28	0.46	0.58
ADM [34]	0.04	0.07	0.09	0.25	0.49
Proposed	**0.08**	0.05	0.04	**0.84**	**0.80**
Poisson					
MLE [21]	0.02	0.03	0.06	0.18	0.34
VMAP [22]	0.03	0.05	0.26	0.29	0.40
BHE [27]	0.05	0.05	0.28	0.47	0.53
SCA [28]	**0.74**	0.60	0.53	0.60	0.44
BMM [29]	0.01	0.27	0.27	0.44	0.61
HBN [30]	0.50	0.48	0.46	0.40	0.52
VBA[33]	0.07	0.21	0.29	0.49	0.56
ADM [34]	0.48	0.52	0.39	0.41	0.59
Proposed	**0.74**	**0.73**	**0.60**	**0.90**	**0.82**

TABLE 13. a. Variation in PSNR w.r.t. variance under different noise distributions for average of image sets at noise level 20dB. b. Variation in PSNR/SSIM w.r.t. variance under different noise distributions for average of image sets at noise level 40dB.

(a)

Variance	0.01	0.02	0.04	0.05
Gaussian				
MLE [21]	33.25	34.25	32.43	32.01
VMAP [22]	35.26	34.20	32.64	31.96
BHE [27]	32.47	32.46	31.13	30.68
SCA [28]	52.63	52.10	51.32	50.98
BMM [29]	52.76	52.00	51.01	50.02
HBN [30]	51.23	51.23	50.57	**50.34**
VBA[33]	36.37	34.82	32.79	30.76
ADM [34]	52.86	53.37	52.44	52.23
Proposed	**53.88**	**52.23**	**51.47**	**50.34**
Gamma				
MLE [21]	41.04	42.28	40.03	39.51
VMAP [22]	43.54	42.23	40.30	39.46
BHE [27]	40.08	40.08	38.44	37.88
SCA [28]	49.86	48.96	47.64	47.07
BMM [29]	50.08	48.79	47.12	45.44
HBN [30]	47.49	47.49	46.36	**45.98**
VBA[33]	44.92	42.99	40.48	37.98
ADM [34]	49.31	50.18	48.60	48.23
Proposed	**51.97**	**49.18**	**47.88**	**45.98**
Poisson				
MLE [21]	39.57	36.05	35.05	31.68
VMAP [22]	39.97	32.09	31.93	30.69
BHE [27]	41.53	40.98	33.38	33.68
SCA [28]	44.99	43.02	42.98	42.67
BMM [29]	45.35	45.55	44.02	43.90
HBN [30]	45.38	45.25	43.35	**43.42**
VBA[33]	42.38	43.23	36.96	36.46
ADM [34]	45.97	45.07	44.81	43.95
Proposed	**45.92**	**45.87**	**44.76**	43.28

(b)

Variance	0.01	0.02	0.04	0.05
Gaussian				
MLE [21]	36.23	36.01	24.89	20.23
VMAP [22]	36.72	32.98	28.88	20.87
BHE [27]	39.87	38.35	37.83	36.23
SCA [28]	44.87	43.98	42.88	**41.87**
BMM [29]	44.99	43.01	42.23	41.43
HBN [30]	44.88	43.36	42.82	41.21
VBA[33]	37.88	32.78	28.91	26.04
ADM [34]	45.29	45.07	42.90	41.20
Proposed	**45.01**	**44.09**	**43.49**	41.43
Gamma				
MLE [21]	36.64	33.38	32.45	29.34
VMAP [22]	37.01	29.72	29.56	28.42
BHE [27]	38.45	37.94	30.91	31.19
SCA [28]	36.92	33.59	33.52	32.99
BMM [29]	37.52	37.87	35.28	35.07
HBN [30]	37.58	37.35	35.13	**35.26**
VBA[33]	39.24	40.02	34.22	33.76
ADM [34]	37.63	36.11	35.68	34.21
Proposed	**38.50**	38.41	**36.53**	34.03
Poisson				
MLE [21]	34.20	33.38	25.53	19.39
VMAP [22]	32.56	33.27	29.20	25.45
BHE [27]	36.58	30.95	28.97	23.01
SCA [28]	36.72	35.21	33.35	**31.64**
BMM [29]	36.92	33.57	32.25	30.90
HBN [30]	36.73	34.15	33.25	30.52
VBA[33]	34.83	30.38	27.43	24.40
ADM [34]	36.50	36.11	32.43	29.55
Proposed	**36.95**	**36.45**	**33.65**	30.89

small for large image sizes and vice versa. The value of root means square error also reduces for large image size. The efficiency of the estimate is analyzed in terms of bias. As bias reduces the efficiency of estimate improves. We have examined the effect of normal priors on the estimates. The precision of the estimate improves by using a good set of priors so that a smaller bias and a smaller RMSE are attained.

Tables 8–10 presents the performance results of different algorithms in terms of performance measures i.e. PSNR, Quality Index, Entropy, run time in seconds, and Correlation coefficient. These performance measures have been evaluated for 20*dB* and 40*dB* of noise levels for Gaussian, Gamma, and Poisson noise cases respectively. The proposed algorithms show a high PSNR value for a low level of noise densities. This means that the image features are well preserved using the proposed method. Moreover, it is observed from Tables 8–10 that the results of the proposed algorithm are compared with [28] at a high level of noise density. This convergence of the proposed algorithm is due to the fact that with an increase in noise density there is an increase in the probability of occurrence of noisy pixels which results in counting more noisy pixels than the central pixel. Because less noisy pixels contribute to maximum likelihood estimation. Moreover, the pixels with high PSNR value tend to have more useful information than the pixels with low PSNR value.

Various statistical parameters have been used in this paper to analyse different denoising algorithms. One of such parameters is Entropy. It is a metric that evaluates the information content of any image. When entropy takes higher values the information content of the image increases which improves the performance. The proposed method yields better qualitative results as compared to various existing methods [21], [22], [27]–[30], [33], and [34]. Another performance metric is Average Correlation which computes the degree of correlation between output and input images. Tables 8–10 also present the execution time in seconds for various methods and it is observed that the proposed algorithm has comparable execution time in comparison to [28], [29].

Table 11a and Table 11b present variation in PSNR w.r.t. average pixel intensity under different noise distributions for an average of image sets at noise level 20dB and 40 *dB* respectively. Table 12a and Table 12b present variation in SSIM w.r.t. average pixel intensity under different noise distributions for an average of image sets at noise level 20dB and 40*dB* respectively. When the noise-free image and denoised image are alike then the value of RMSE becomes zero which improves the PSNR value. On the other hand, when the similarity between the noise-free image and denoised image reduces then the PSNR value also reduces. Table 13a and 13b present variation in PSNR w.r.t. variance under different noise distributions for an average of image sets at noise level 20dB and 40 *dB* respectively. It is observed that for large values of variance the PSNR

reduces which assesses the performance of the proposed method.

VI. CONCLUSION

There exist various applications of image denoising such as medical imaging, remote sensing, biometrics and forensics, industrial and agricultural automation, etc. In this paper, the spatial resolution of the image has improved using the proposed image denoising method. Therefore, the proposed method is proven to be capable to preserve the original spectral content of any image. The performance results have been evaluated in terms of qualitative and quantitative results which include both spectral and spatial properties. The proposed method is based on an exponential family of distributions whose priors have been estimated w.r.t. the parameter of interest for Gaussian, Gamma and Poisson noise cases. The proposed method has shown better results about the denoising method so that the noise can be removed from the image by preserving image details. The noise reduction in the image is achieved by using conditional likelihood and wavelet transformation-based minimization technique. The accuracy and reliability of the proposed methods is validated by analyzing priors and posteriors distribution. The proposed method presents an accurate noise model whereas the existing methods just present noise distribution in the pixel intensity domain. The numerical results present a quantitative comparison of the proposed method with other conventional methods.

Any single denoising algorithm may not be able to exhibit the desired level of applicability. Therefore in the future, we would combine various methods in different domains to harness the attributes of various domains while overcoming limitations of each other. For future work, we will also explore real-life noises because the real noises are much more complex than the considered noise models. It has been observed that the proposed method leaves a residual noise and may not be able to sustain the optimal performance at extremely higher noise levels. However, within the standard bounds of noise levels, the proposed method holds performance consistency, high visual quality, and preservation of fine feature details.

REFERENCES

[1] L. Fan, F. Zhang, H. Fan, and C. Zhang, "Brief review of image denoising techniques," *Vis. Comput. Ind.*, vol. 2, no. 1, Jul. 2019, Art. no. 7.

[2] Y. Wang, M. Shi, S. You, and C. Xu, "DCT inspired feature transform for image retrieval and reconstruction," *IEEE Trans. Image Process.*, vol. 25, pp. 4406–4420, 2016.

[3] A. Dogra, B. Goyal, S. Agrawal, and C. K. Ahuja, "Efficient fusion of osseous and vascular details in wavelet domain," *Pattern Recognit. Lett.*, vol. 94, pp. 189–193, Jul. 2017.

[4] X. Wang, D. Zhang, and X. Guo, "A novel image recovery method based on discrete cosine transform and matched blocks," *Nonlinear Dyn.*, vol. 73, no. 3, pp. 1945–1954, Apr. 2013.

[5] I. J. Myung, "Tutorial on maximum likelihood estimation," *J. Math. Psychol.*, vol. 47, no. 1, pp. 90–100, Feb. 2003.

[6] R. E. Neapolitan, *Learning Bayesian Networks*. Upper Saddle River, NJ, USA: Prentice-Hall, 2004.

[7] M. Makitalo and A. Foi, "Poisson-Gaussian denoising using the exact unbiased inverse of the generalized Anscombe transformation," in *Proc. IEEE Int. Conf. Acoust., Speech Signal Process. (ICASSP)*, Kyoto, Japan, Mar. 2012, pp. 1081–1084.

[8] J. Zhang and K. Hirakawa, "Improved denoising via Poisson mixture modeling of image sensor noise," *IEEE Trans. Image Process.*, vol. 26, pp. 1565–1578, 2017.

[9] K. Hirakawa and P. J. Wolfe, "Skellam shrinkage: Wavelet-based intensity estimation for inhomogeneous Poisson data," *IEEE Trans. Inf. Theory*, vol. 58, no. 2, pp. 1080–1093, Feb. 2012.

[10] A. Foi, M. Trimeche, V. Katkovnik, and K. Egiazarian, "Practical Poissonian-Gaussian noise modeling and fitting for single-image raw-data," *IEEE Trans. Image Process.*, vol. 17, no. 10, pp. 1737–1754, Oct. 2008.

[11] Z. Xia, X. Wang, C. Wang, and C. Zhang, "Subpixel-based accurate and fast dynamic tumor image recognition," *J. Med. Imag. Health Informat.*, vol. 8, no. 5, pp. 925–931, Jun. 2018.

[12] G. Yu, G. Sapiro, and S. Mallat, "Solving inverse problems with piecewise linear estimators: From Gaussian mixture models to structured sparsity," *IEEE Trans. Image Process.*, vol. 21, pp. 2481–2499, 2012.

[13] J. A. Guerrero-Colon, L. Mancera, and J. Portilla, "Image restoration using space-variant Gaussian scale mixtures in overcomplete pyramids," *IEEE Trans. Image Process.*, vol. 17, pp. 27–41, 2008.

[14] D. Gleich and M. Datcu, "Wavelet-based despeckling of SAR images using Gauss–Markov random fields," *IEEE Trans. Geosci. Remote Sens.*, vol. 45, no. 12, pp. 4127–4143, Dec. 2007.

[15] F. Argenti, T. Bianchi, A. Lapini, and L. Alparone, "Fast MAP despeckling based on Laplacian–Gaussian modeling of wavelet coefficients," *IEEE Geosci. Remote Sens. Lett.*, vol. 9, no. 1, pp. 13–17, Jan. 2012.

[16] J. Settle, "On the effect of variable endmember spectra in the linear mixture model," *IEEE Trans. Geosci. Remote Sens.*, vol. 44, no. 2, pp. 389–396, Feb. 2006.

[17] A. Levin, B. Nadler, F. Durand, and W. T. Freeman, "Patch complexity, finite pixel correlations and optimal denoising," in *Proc. 12th Eur. Comput. Vis. (ECCV)*, vol. 7576, Oct. 2012, pp. 73–86.

[18] A. Levin and B. Nadler, "Natural image denoising: Optimality and inherent bounds," in *Proc. IEEE Conf. Comput. Vis. Pattern Recognit. (CVPR)*, Jun. 2011, pp. 2833–2840.

[19] B. Goossens, A. Pizurica, and W. Philips, "Image denoising using mixtures of projected Gaussian scale mixtures," *IEEE Trans. Image Process.*, vol. 18, pp. 1689–1702, 2009.

[20] C.-A. Deledalle, L. Denis, and F. Tupin, "Iterative weighted maximum likelihood denoising with probabilistic patch-based weights," *IEEE Trans. Image Process.*, vol. 18, pp. 2661–2672, 2009.

[21] J. Sijbers and A. J. den Dekker, "Maximum likelihood estimation of signal amplitude and noise variance from MR data," *Magn. Reson. Med.*, vol. 51, no. 3, pp. 586–594, 2004.

[22] A. B. Hamza and H. Krim, "A variational approach to maximum a posteriori estimation for image denoising," in *Proc. Int. Workshop Energy Minimization Methods Comput. Vis. Pattern Recognit.* (Lecture Notes in Computer Science), vol. 2134. Berlin, Germany: Springer-Verlag, 2001, pp. 19–34.

[23] S. Lyu and E. P. Simoncelli, "Modeling multiscale subbands of photographic images with fields of Gaussian scale mixtures," *IEEE Trans. Pattern Anal. Mach. Intell.*, vol. 31, no. 4, pp. 693–706, Apr. 2009.

[24] D. Titterington, A. Smith, and U. Makov, *Statistical Analysis of Finite Mixture Distributions*. Hoboken, NJ, USA: Wiley, 1985.

[25] A. Blake and A. Zisserman, *Visual Reconstruction*. Cambridge, MA, USA: MIT Press, 1987.

[26] L. Boubchir and J. M. Fadili, "A closed-form nonparametric Bayesian estimator in the wavelet domain of images using an approximate α-stable prior," *Pattern Recognit. Lett.*, vol. 27, no. 12, pp. 1370–1382, Sep. 2006.

[27] Y. Wan and R. Nowak, "Bayesian multiscale approach to joint image restoration and edge detection," *Proc. SPIE Wavelet Appl. Signal Image Process.*, vol. 3813, pp. 73–84, Oct. 1999.

[28] T. Kasetkasem, M. K. Arora, P. K. Varshney, and V. Areekul, "Improving subpixel classification by incorporating prior information in linear mixture models," *IEEE Trans. Geosci. Remote Sens.*, vol. 49, no. 3, pp. 1001–1013, Mar. 2011.

[29] H.-C. Li, W. Hong, Y.-R. Wu, and P.-Z. Fan, "Bayesian wavelet shrinkage with heterogeneity-adaptive threshold for SAR image despeckling based on generalized gamma distribution," *IEEE Trans. Geosci. Remote Sens.*, vol. 51, no. 4, pp. 2388–2402, Apr. 2013.

[30] J. Ho and W.-L. Hwang, "Wavelet Bayesian network image denoising," *IEEE Trans. Image Process.*, vol. 22, no. 4, pp. 1277–1290, Apr. 2013.

[31] H.-C. Li, W. Hong, Y.-R. Wu, and P.-Z. Fan, "On the empirical-statistical modeling of SAR images with generalized gamma distribution," *IEEE J. Sel. Topics Signal Process.*, vol. 5, no. 3, pp. 386–397, Jun. 2011.

[32] E. Chouzenoux, A. Jezierska, J.-C. Pesquet, and H. Talbot, "A convex approach for image restoration with exact Poisson-Gaussian likelihood," *SIAM J. Imag. Sci.*, vol. 8, no. 4, pp. 2662–2682, Jan. 2015.

[33] Y. Marnissi, Y. Zheng, E. Chouzenoux, and J.-C. Pesquet, "A variational Bayesian approach for image restoration—Application to image deblurring with Poisson–Gaussian noise," *IEEE Trans. Comput. Imag.*, vol. 3, no. 4, pp. 722–737, Dec. 2017.

[34] M. Ghulyani and M. Arigovindan, "Fast roughness minimizing image restoration under mixed Poisson–Gaussian noise," *IEEE Trans. Image Process.*, vol. 30, pp. 134–149, 2021.

[35] A. Nandal, V. Bhaskar, and A. Dhaka, "Contrast-based image enhancement algorithm using grey-scale and colour space," *IET Signal Process.*, vol. 12, no. 4, pp. 514–521, Jun. 2018.

[36] A. Nandal and V. Bhaskar, "Enhanced image fusion using directive contrast with higher-order approximation," *IET Signal Process.*, vol. 12, no. 4, pp. 383–393, Jun. 2018.

[37] Y. Liang, F. He, and X. Zeng, "3D mesh simplification with feature preservation based on whale optimization algorithm and differential evolution," *Integr. Comput.-Aided Eng.*, vol. 27, no. 4, pp. 417–435, 2020.

[38] D. Goldfarb and W. Yin, "Second-order cone programming methods for total variation-based image restoration," *SIAM J. Sci. Comput.*, vol. 27, no. 2, pp. 622–645, 2005.

[39] D.-Q. Chen, H. Zhang, and L.-Z. Cheng, "A fast fixed point algorithm for total variation deblurring and segmentation," *J. Math. Imag. Vis.*, vol. 43, no. 3, pp. 167–179, Jul. 2012.

[40] H. Woo and S. Yun, "Proximal linearized alternating direction method for multiplicative denoising," *SIAM J. Sci. Comput.*, vol. 35, no. 2, pp. B336–B358, Jan. 2013.

[41] H. Li, F. He, Y. Chen, and Y. Pan, "MLFS-CCDE: Multi-objective large-scale feature selection by cooperative coevolutionary differential evolution," *Memetic Comput.*, vol. 13, no. 1, pp. 1–18, Mar. 2021.

[42] L. Zhou, A. Dhaka, H. Malik, A. Nandal, S. Singh, and T. Wu, "An optimal higher order likelihood distribution based approach for strong edge and high contrast restoration," *IEEE Access*, vol. 9, pp. 109012–109024, 2021.

[43] A. Nandal, A. Dhaka, H. Gamboa-Rosales, N. Marina, J. I. Galvan-Tejada, C. E. Galvan-Tejada, A. Moreno-Baez, J. M. Celaya-Padilla, and H. Luna-Garcia, "Sensitivity and variability analysis for image denoising using maximum likelihood estimation of exponential distribution," *Circuits, Syst., Signal Process.*, vol. 37, no. 9, pp. 3903–3926, Sep. 2018.

[44] S. Singh and M. Fozdar, "Optimal bidding strategy with the inclusion of wind power supplier in an emerging power market," *IET Gener., Transmiss. Distrib.*, vol. 13, no. 10, pp. 1914–1922, May 2019.

[45] R. Hogg, J. McKean, and A. Craig, *Introduction to Mathematical Statistics*. Englewood Cliffs, NJ, USA: Prentice-Hall, 2005.

[46] B. L. Xiong, M. C. Jing, and G. Y. Kuang, "A change detection measure based on a likelihood ratio and statistical properties of SAR intensity images," *Remote Sens. Lett.*, vol. 3, pp. 267–275, Oct. 2012.

[47] Y. Chen, W. Feng, and R. Ranftl, "A higher-order MRF based variational model for multiplicative noise reduction," *IEEE Signal Process. Lett.*, vol. 21, no. 11, pp. 1370–1374, Jul. 2014.

[48] R. Nowak and E. Kolaczyk, "A Bayesian multiscale framework for Poisson inverse problems," *IEEE Trans. Inf. Theory*, vol. 46, pp. 1811–1825, 2000.

[49] M. Lebrun, A. Buades, and J.-M. Morel, "A nonlocal Bayesian image denoising algorithm," *SIAM J. Imag. Sci.*, vol. 6, no. 3, pp. 1665–1688, 2013.

[50] T. Le, T. Chartrand, and T. J. Asaki, "A variational approach to reconstructing images corrupted by Poisson noise," *J. Math. Imag. Vis.*, vol. 27, no. 3, pp. 257–263, Apr. 2007.

[51] S. Gu, L. Zhang, W. Zuo, and X. Feng, "Weighted nuclear norm minimization with application to image denoising," in *Proc. IEEE Int. Conf. Comput. Vis. Pattern Recognit.*, Columbus, OH, USA, Jun. 2014, pp. 2862–2869.

[52] L. Zhang, L. Zhang, X. Mou, and D. Zhang, "FSIM: A feature similarity index for image quality assessment," *IEEE Trans. Image Process.*, vol. 20, pp. 2378–2386, 2011.

[53] Z. Wang, A. C. Bovik, H. R. Sheikh, and E. P. Simoncelli, "Image quality assessment: From error visibility to structural similarity," *IEEE Trans. Image Process.*, vol. 13, pp. 600–612, 2004.

[54] *Website*. Accessed: Aug. 15, 2021. [Online]. Available: http://vision.middlebury.edu/stereo/data/

ARVIND DHAKA received the Ph.D. degree in computer science and engineering from NIT Hamirpur, India (an institute of national importance), in 2018. Since 2018, he has been working as an Assistant Professor with the Department of Computer and Communication Engineering, Manipal University Jaipur. His research interests include wireless communication, wireless sensor networks, *ad-hoc* networks, medical image processing, machine leaning, and deep learning in image processing.

AMITA NANDAL received the Ph.D. degree in electronics and communication engineering from SRM University, Chennai, in 2014. Since 2018, she has been working as an Associate Professor with the Department of Computer and Communication Engineering, Manipal University Jaipur. Her research interests include digital signal processing, machine learning and deep learning for medical image processing, wireless communication, circuits systems, and FPGA implementation.

HAMURABI GAMBOA ROSALES received the bachelor's degree in electronics and communications engineering from the Faculty of Engineering, University of Guadalajara, in 2000, the master's degree in electrical engineering from the University of Guanajuato, in 2003, with a focus on digital signal processing, and the Ph.D. degree in voice processing from the Technical University of Dresden, Germany, in 2010. He is currently working as a Professor and a Researcher with the Academic Unit of Electrical Engineering, Autonomous University of Zacatecas, Mexico, in the area of research digital signal processing.

HASMAT MALIK (Senior Member, IEEE) received the M.Tech. degree in electrical engineering from the National Institute of Technology (NIT) Hamirpur, Himachal Pradesh, India, and the Ph.D. degree in electrical engineering from the Indian Institute of Technology (IIT), Delhi, India. He has served as an Assistant Professor for more than five years at the Division of Instrumentation and Control Engineering, Netaji Subhas Institute of Technology (NSIT), Dwarka, Delhi. He is currently a Chartered Engineer (C.Eng.) and a Professional Engineer (P.Eng.). He has been a Research Fellow with Berkeley Education Alliance for Research in Singapore (BEARS), a research center of the University of California, Berkeley, University Town, National University of Singapore (NUS), Singapore, since January 2019. He has published widely in international journals and conferences. His research findings related to intelligent data analytics, artificial intelligence, machine learning applications in power systems, power apparatus, smart building and automation, smart grid, forecasting, prediction, and renewable energy sources. He has authored/coauthored more than 100 research papers and eight books and 13 chapters in nine other books, published by IEEE, Springer, and Elsevier. He has supervised 23 PG students. His principal area of research interests include artificial intelligence, machine learning and big-data analytics for renewable energy, smart building and automation, condition monitoring, and online fault detection and diagnosis (FDD). He is a member of the Computer Science Teachers Association (CSTA), the Association for Computing Machinery (ACM) EIG, the Institution of Engineering and Technology (IET), U.K., and Mir Labs, Asia. He is a Life Member of the Indian Society for Technical Education (ISTE), the Institution of Engineers (IEI), India, and the International Society for Research and Development (ISRD), London. He is a fellow of the Institution of Electronics and Telecommunication Engineering (IETE). He received the POSOCO Power System Award (PPSA-2017) for his Ph.D. work for research and innovation in the area of power systems. He also received the Best Research Papers Awards from IEEE INDICON-2015 and the Full Registration Fee Award from IEEE SSD-2012, Germany.

FRANCISCO ENELDO LOPEZ MONTEAGUDO is currently a Senior Research Professor with the School of Electrical Engineering, Autonomous University of Zacatecas, Mexico. He is a member of the National System of Researchers with the Desirable Profile PRODEP.

MONICA I. MARTINEZ-ACUNA received the Ph.D. degree in environmental sciences from the Autonomous University of San Luis Potosí (UASLP). She is currently a Professor with the Faculty of Chemical Sciences, Autonomous University of Zacatecas (UAZ). Her project is about geographic distribution of environmental risks, social determinants, and their contribution to the global burden of acute lymphoblastic leukemia in Mexico. Her research interests include evaluation of environmental risks, spatial environmental epidemiology, children's environmental health, and characterization of natural products.

SATYENDRA SINGH (Member, IEEE) received the bachelor's (B.E.) degree in electrical engineering from the Government Engineering College Bikaner, Rajasthan, India, in 2008, the master's degree in power systems from the National Institute of Technology (NIT), Hamirpur Himachal Pradesh, India, in 2011, and the Ph.D. degree in electrical engineering from the Malaviya National Institute of Technology (MNIT), Jaipur, Rajasthan, in 2019. He is currently working as an Assistant Professor with the School of Electrical Skills, Bhartiya Skill Development University, Jaipur. His research interests include power systems, power system economics, electricity market, renewable energy modeling, FACTs devices, multi-agent systems, and nature-inspired algorithms.